856

VALIDITY OF RUTHERFORD SCATTERING

by

Said A. Agamy

PART A: MCMASTER INDUSTRIAL PROJECT*

A project* report submitted in partial fulfillment of the
requirements for the degree of
Master of Engineering

Department of Engineering Physics
McMaster University
Hamilton, Ontario
September, 1973

* One of two project reports. The other one is designated PART B:
MCMASTER ON-CAMPUS PROJECT

Said Agamy

McMaster University
Hamilton, Ontario

TITLE: VALIDITY OF RUTHERFORD SCATTERING

SUPERVISOR: Dr. J.A. Davies

NUMBER OF PAGES: 48

CONTENTS

ABSTRACT

The purpose of this report is to study the validity of the Rutherford Scattering Law. Both the angular and energy dependence of the scattering cross-section are checked, also comparison between the absolute cross-section determined experimentally and the theoretical cross-section is made.

Here we study the scattering of helium and oxygen ions with energies varying from 0.5 to 2.0 MeV from thin bismuth targets made by implanting 40 keV bismuth ions in low Z(silicon) substrate to doses of 10^{16} ions/cm^2. The implantation process was made on the Isotope Separator and the scattering experiments were made on the Van-de-Graff accelerator of the SSS branch of the AECL. The scattering angles considered here range from 90° to 160° and a special geometrical arrangement was used to enable us to measure the scattering angle accurately. Also the report contains a brief description of the different sources of errors during target preparation (implantations) and the scattering experiments.

ACKNOWLEDGMENT

I wish to express my deep gratitude and great thanks to Professor J.A. Davies for his continuous help and assistance during the course of this work. Also, I would like to thank the staff of SSS of the AECL for the different discussions made.

Finally, I thank O.M. Westcott for doing the required implantations, J. Lori and D. Lanteigne for their assistance on the Van-de-Graff during the scattering experiments, and D. Dixon for making the desired arrangements in the machine shop.

Said Agamy

CHAPTER 1

INTRODUCTION

The elastic scattering of ions and atoms is widely used now as an analytical probe in the field of Solid State Science. In such applications using nuclear backscattering, it is generally assumed that the Rutherford cross-section is valid. However, not much work was done to verify the accuracy of these cross-sections experimentally. Only few papers were published for the study of the scattering of low Z ions, and one of these is Rutherford's own work.[1]

There are two different extremes in the study of the validity of Rutherford law. The first is the scattering at large separation distance between the bombarding ion and the scattering atom where the screening effect of orbital electrons is large (separation distance of the order of the electronic orbit diameter, i.e. $\sim 10^{-8}$ cm). The second is the scattering at very small separation distance(of the order of the nucleus diameter, i.e. $\sim 10^{-12}$cm) where the bombarding ion penetrates the nuclear barrier and we have anomalous scattering. The separation distance is proportional to the value of $\left(\frac{Z_1 Z_2}{E \sin^2 \theta}\right)$ and so this is the parameter that controls the separation distance.

Recently H.H. Anderson et al[2] studied the differential cross-section for elastic scattering of 300-2000 keV H^+ and 300-500 keV He^+ and Li^+ through 3°-15° by gold target. They used thin (34-220 mg/cm^2) vacuum-deposited polycrystalline gold foils. From the energies and scattering

angles they considered, it is clear that they studied scattering at large separation distances. On the other hand, J.F. Ziegler and J.E.E. Baglin[2] studied the elastic backscattering of He^+ from a variety of thin films containing Si, Al, O, and N for He^+ energies ranging from 1-2.5 MeV. In this range, the helium ions are able to penetrate the nuclear barrier and will be affected by the nuclear forces beside the usual Coulomb field.

In this report, we study the elastic scattering of 500-2000 keV He^+ and 1000 keV O^+ through 90°-160° by bismuth targets. So we will cover the range of separation distances between the above two extremes.

In the previous work by Anderson, and by Ziegler, they used self-supporting thin targets; the thickness of these targets is hard to be measured accurately. So, instead of that technique, we produced a thin Bi target by uniformly implanting Bi ions in a low Z (silicon) substrate; the Bi ions penetrate the substrate to a certain depth which is known. Since in the backscattered spectra of both He^+ and O^+ ions from these targets we have a clear energy separation between the Bi peak and the edge of Si spectrum. Therefore by fixing the window of a single channel analyser, we can observe the counts due to scattering from Bi alone. Knowing the scattering angle and the energy of the incident ions, we can examine the validity of both the angular and energy dependence of the Rutherford law. Also, from the geometrical arrangement of the target and detector, we can get the absolute value of the scattering cross-section at each energy and scattering angle and compare this with the theoretically calculated cross-sections.

In Chapter 2, the basic theoretical treatment of the Rutherford scattering is discussed, and also the method followed in determining the scattering cross-section from the experimental data and in checking the validity of the angular and energy dependence of the observed counts. In Chapter 3, we explain the method for preparing our Bi targets and the sources of error that might occur during the implantation process, also the corrections required in our calculations due to the finite penetration of Bi ions through the Si targets. This latter point involves calculating (a) the projected range of the Bi ions and (b) the energy lost by helium and oxygen ions in traversing the Si layer to the depth of the Bi atoms during the subsequent scattering experiments. In Chaper 4, the main scattering experiment is discussed in detail with the description of the experimental arrangement and the reason for choosing this arrangement. The ion current measurements are discussed, and the explanation of the technique used in making our measurements. Also in this Chapter, we discuss the different sources of error and the experimental work done to check their effect on our results. Finally, in Chapter 5, we make a tabulation of the complete analysed experimental data and the discussions and comments on these results concerning angular and energy dependence, absolute magnitude of scattering cross-section compared with theoretical value and the reproducibility of the output we obtained.

CHAPTER 2

RUTHERFORD SCATTERING

In this Chapter, we include the basic theoretical treatment of the Rutherford scattering. From the interaction yield, it is possible to find the value of the experimentally determined scattering cross-section. A brief description for the corrections required due to the energy loss by ions in penetrating the silicon layer until it reaches the bismuth atoms locations. Also included is the procedure required to check the angular and energy dependence of the scattering cross-section.

2.1 Rutherford Law

In this section only the main equations that will be used are presented without complete mathematical derivations. The complete theoretical treatment can be found in most nuclear physics textbooks.[4]

The relation between the scattering angle θ in the lab. system an the scattering angle Θ in the C.M. system is given by

$$\sin(\Theta - \theta) = \frac{M_1}{M_2} \sin\theta \qquad (2\text{-}1)$$

where M_1 and M_2 are the masses of projectile and target atom respectively.

The collision diameter b, which equals the closest distance of approach in a head-on collision,is expressed as

$$b = \frac{2|Z_1 Z_2|\ e^2}{M_o\ V^2} \qquad (2.2)$$

where Z_1 and Z_2 are the atomic numbers of projectile and target respectively and $|Z_1 Z_2|$ is the absolute value of $Z_1 Z_2$, e is the electronic charge, V is the projectile initial velocity in the lab. coordinates, and M_o is the reduced mass of the system of particles and is defined by

$$M_o = \frac{M_1 M_2}{M_1 + M_2} \qquad (2\text{-}3)$$

Substituting the value of M_o and putting $\gamma = M_1/M_2$ in Equation (2-2), therefore

$$b = \frac{|Z_1 Z_2|e^2}{E}\left(\frac{M_1 + M_2}{M_2}\right) = \frac{|Z_1 Z_2|e^2}{E}\ (1 + \gamma) \qquad (2\text{-}4)$$

where E is the initial projectile energy = $\frac{1}{2} M_1\ V^2$.

The impact parameter x in terms of the collision diameter and the C.M. scattering angle is given by

$$x = \frac{b}{2} \cot\ \frac{\Theta}{2} \qquad (2\text{-}5)$$

The differential cross-section for scattering of M_1 into the solid angle $d\omega = 2\pi \sin\theta\ d\theta$ in the lab. coordinates will be called $d\sigma \equiv \xi_o(\theta)d\omega$. The fraction of the incident particles which are scattered by a very thin foil containing N target praticles M_2 per square centimeter is $N\ \xi_o(\theta)\ d\omega$. These are the same particles which, in the C.M. coordinates, are scattered in the solid angle $d\Omega = 2\pi \sin\Theta\ d\Theta$

If the differential cross-section, $d\sigma$, is called $\xi_o(\Theta)\ d\Omega$ in the C.M. coordinates, then

$$\frac{d\sigma}{2\pi} = \xi_o(\theta)\, \sin\theta d\theta = \xi_o(\Theta)\, \sin\Theta\, d\Theta \qquad (2\text{-}6)$$

The differential cross-section $\xi_o(\Theta)\, d\Omega$ for an impact parameter between x and x + dx is simply the area of a ring of radius x, and width dx, which is $2\pi x dx$. Then from Equation (2-5), we have

$$d\sigma \equiv \xi_o(\Theta)\, d\Omega = 2\pi x dx = 2\pi\left(\frac{b}{2}\cot\frac{\Theta}{2}\right)\frac{b}{2}\csc^2\frac{\Theta}{2}\,\frac{d\Theta}{2}$$

$$= \pi\frac{b^2}{4}\,\frac{\cos(\Theta/2)}{\sin^3(\Theta/2)}\,d\Theta = \frac{b^2}{16}\,\frac{1}{\sin^4(\Theta/2)}\,d\Omega \qquad (2\text{-}7)$$

Substituting the value of the collision diameter b from Equation (2-4), we get

$$\frac{d\sigma}{d\Omega} = \left(\frac{Z_1 Z_2 e^2}{4E}\right)^2 (1+\gamma)\,\frac{1}{\sin^4(\Theta/2)}$$

$$= 1.2926 \times 10^{-27}\left(\frac{Z_1 Z_2}{E}\right)^2 (1+\gamma)\,\frac{1}{\sin^4(\Theta/2)}\ \text{cm}^2/\text{sr}. \qquad (2\text{-}8)$$

in Equation (2-8), the energy E is in MeV.

This cross-section can be transposed to the lab. coordinates when γ, i.e. M_1/M_2, and hence the relationship between θ and Θ, is known from Equation (2-1). In the general case, we have for the differential cross-section in the lab. coordinates,

$$d\sigma = \xi_o(\theta)\, d\omega = \xi_o(\Theta)\,\frac{\sin\Theta\, d\Theta}{\sin\theta\, d\theta}\, d\omega \qquad (2\text{-}9)$$

From Equations (2-1), (2-8), and (2-9) we can obtain the following

expression for the differential cross-section in the lab. coordinates,

$$d\sigma = \xi_o(\Theta) \frac{(1 + \gamma^2 + 2\gamma \cos\Theta)^{3/2}}{1 + \gamma \cos\Theta} d\omega$$

$$= 1.2926 \times 10^{-27} \left(\frac{Z_1 Z_2}{E}\right)^2 (1 + \gamma) \frac{1}{\sin^4(\Theta/2)} \left[\frac{(1 + \gamma^2 + 2\gamma \cos\Theta)^{3/2}}{1 + \gamma \cos\Theta}\right] d\omega \quad (2\text{-}10)$$

Actually in our work we will evaluate the value of the scattering cross-section per unit solid angle in the C.M. system theoretically and experimentally and examine the agreement between theory and experiment.

2.2 Interaction Yield

If the number of bombarding ions incident on the target is I_o with incident energy E_o, the yield of backscattered ions at a certain angle θ (in the lab. coordinates) is determined by the scattering cross-section corresponding to this angle and the ion energy at the scattering site E_s. E_s is slightly smaller than E_o, as we will see in the next section. Also, this yield will be proportional to I_o, and to N'(the number of Bi ions per square centimeter, measured perpendicular to the incident beam direction. If ϕ is the angle between the incident beam and the normal to the target, then $N' = N/\cos\phi$, therefore we have

$$I = I_o \frac{N}{\cos\phi} \sigma_{lab.}(E_s, \theta) \quad (2\text{-}11)$$

where $\sigma_{lab.}(E_s, \theta)$ is the microscopic scattering cross-section at energy E_s and scattering angle ϕ in the lab. coordinates.

From Equation (2-9) we can put Equation (2-11) in terms of the C.M. cross-section, therefore

$$I = I_o \frac{N}{\cos\phi} \xi_o(E_s, \Theta) \left[\frac{(1 + \gamma^2 + 2\gamma \cos\Theta)^{3/2}}{1 + \gamma \cos\Theta}\right]\omega \qquad (2\text{-}12)$$

where ω is the solid angle subtended by the detector at the target. Equation (2-12) gives the experimentally determined scattering cross-section per C.M. steradian $\xi_o(E_s, \Theta)$ which, if the Rutherford Law is exactly valid, will be the same as that calculated theoretically from Equation (2-8).

2.3 Energy Loss Correction

In this section, we discuss, qualitatively, the reason for this energy loss correction. The complete evaluation of the magnitude of this loss will be given in Chapter 3.

In this work we are studying the scattering from thin Bi targets made by implanting Bi ions into Si substrates, as will be explained in Chapter 3. Therefore, our scattering process does not occur on the surface of the substrate, but at a depth corresponding to the Bi penetration profile; we must therefore determine the mean projected range of these ions in the Si substrate. On bombarding these targets with high energy ions, such as He^+ and O^+, they lose certain amount of energy in Si layer before reaching the Bi location and being scattered.

Knowing the projected range R_p of the implanted Bi in the Si substrate, the initial energy E_o of the bombarding ion, and its stopping power

S in the Si, the ion energy just before scattering from Bi will be given by

$$E_s = E_o - S.R_p \qquad (2\text{-}13)$$

In calculating the scattering cross-section theoretically from Equation (2-8), we have to substitute the exact value of the energy at the scattering site which is E_s and not E_o.

In practice, we select approximately the required energy E_o from the Van-de-Graff panel, calculate the exact energy at the scattering location E_s from Equation (2-13), and then calculate the theoretical cross-section corresponding to E_s rather than E_o.

2.4 Angular and Energy Dependence

Substituting the theoretical value of $\xi_o(E_s, \Theta)$ in Equation (2-12) from Equation (2-8), we get the following form of the yield equation

$$I = I_o \frac{N}{\cos\phi} \left[1.2926 \times 10^{-27}\left(\frac{Z_1 Z_2}{E_s}\right)^2 (1+\gamma) \frac{1}{\sin^4(\Theta/2)} \left[\frac{(1+\gamma^2+2\gamma\cos\Theta)^{3/2}}{1+\gamma\cos\Theta}\right]\omega \qquad (2\text{-}13)$$

Therefore, for a certain target-projectile combination we have

$$I = C\left(\frac{1}{E_s^2}\right)\left[\frac{1}{\cos\phi} \frac{1}{\sin^4(\Theta/2)} \frac{(1+\gamma^2+2\gamma\cos\Theta)^{3/2}}{(1+\gamma\cos\Theta)}\right] \qquad (2\text{-}14)$$

where C is a constant given by

$$C = 1.2926 \times 10^{-27} I_o N(Z_1 Z_2)^2 (1+\gamma)\omega$$

The Equation (2-14) assumes the validity of Rutherford's Law. Therefore, we can make use of this relation to check both the angular and energy dependence of the Rutherford Law.

For angular dependence we will have a fixed value of energy E_s, therefore the yield equation becomes

$$I = C'\left[\frac{1}{\cos\phi}\ \frac{1}{\sin^4(\theta/2)}\ \frac{(1+\gamma^2+2\gamma\cos\theta)^{3/2}}{(1+\gamma\cos\theta)}\right] \qquad (2\text{-}15)$$

where C' is a constant. So changing the scattering angles and recording the observed counts for each position, from Equation (2-15), we can check to what extent the angular dependence is correct, since dividing the counts observed over the quantity in square brackets should give a constant value for the different scattering angles at fixed energy and the same target-projectile combination.

For energy dependence the same is done except the angular term is constant and we vary the energy E_s. Therefore the rate equation takes the form

$$I = C''\ \frac{1}{E_s^2} \qquad (2\text{-}16)$$

So multiplying the observed number of counts by the square of the corresponding energy at the scattering location E_s, this will be a constant (C'') if the energy dependence is exact.

The scattering experiment was done using different targets and therefore the number of implanted Bi ions per square centimeter, N, will be different. This was done to check the reproducibility of our results. Therefore in checking angular and energy dependence for these runs with

different targets, we have to include the value of N as a variable in our rate equation.

All these calculations are put in the final tabular form in Chapter 5.

CHAPTER 3

HEAVY ION IMPLANTATION

In this Chapter, the preparation of thin Bi targets is explained. In Chapter 2, we discussed the need to evaluate the finite penetration of the implanted ions through the Si substrate and the energy lost by the bombarding ions in the scattering experiments until it reachs the Bi layer. Here we make the complete calculations for the Bi ions range and the energy lost by the He^+ and O^+, which are the only ions used in our scattering experiments, in the Si layer. At the end of the Chapter, various sources of error in the implantation process will also be discussed.

3.1 Target Preparation

It is hard to make a self-supporting uniform thin target, and it is difficult to measure its thickness accurately. To avoid these difficulties we used a different technique in preparing our targets. This was done by implantation of our heavy ion (Bi) in a low z(silicon) substrate, and therefore by uniform implantation we obtain a thin Bi target for our scattering experiments.

The Bi ions were produced by evaporating Bi metal and then accelerating these ions to the implantation potential of 40 kV, the beam is deflected by the analyzing magnet in the isotope separator and is focused as a vertical line at the target position. To achieve uniform implanation, the beam is

swept evenly in the horizontal direction over the area of the target defined by the beam defining aperture. The current integrator connected to the target holder records the absolute number of microcoulombs of beam hitting the target.

For our scattering experiments we made two different targets with different implanted doses, as follows

Target Number	Implanted Dose ($\mu c/cm^2$)	Implanted Dose (Ions/cm^2)	Target Chamber Pressure (Torr)
1	316	1.9687×10^{15}	1×10^{-6}
2	1625.5	1.0127×10^{16}	2×10^{-6}

3.2 Projected Range of Implanted Ions

The implanted Bi ions penetrate the Si substrate and do not stay right on the surface as we mentioned in section 2.3. Calculation of the projected range of these implanted ions is necessary for the energy loss evaluation in the next section.

In our calculations we will make use of the tables made by K.B. Winterbon.[5] For Bi-209 penetration through Si-28, we have from table (I), p.12

$\varepsilon = 0.000664$ per keV

$\rho = 0.0249$ per $\mu g/cm^2$

$k = 0.1158$

where ε, ρ, and k are dimensionless energy, range, and electronic stopping

parameters respectively.

For our implantations, the Bi ions energy was 40 keV, therefore

$$\varepsilon = 0.000664 \times 40 = 0.02656$$

and by interpolations in table (II), p.28, we have

$$\text{for } \varepsilon = 0.02656 \text{ and } k = 0.1158, \rho = 0.1328$$

Since $\rho = 0.0249\ R_{total}$

where R_{total} is the total range, therefore

$$R_{total} = \frac{0.1328}{0.0249} = 5.337 \quad \mu g/cm^2$$

The relation between the projected range R_p and the total range R_{total} is given by[6]

$$\frac{R_p}{R_{total}} = \left(1 + \frac{M_2}{3M_1}\right)^{-1}$$

here $M_1 \equiv$ mass of bombarding ion (Bi) = 209,

$M_2 \equiv$ mass of bombarded substrate (Si) = 28

Therefore

$$R_p = 0.96\ R_{total}$$

$$= 0.96 \times 5.337 = 5.110 \quad \mu g/cm^2$$

Since Si density - 2.42 gm/cm^2, therefore

$$R_p = \frac{5.11 \times 10^{-6}}{2.42} \simeq 200°A$$

i.e. The projected range of 40 keV Bi ions in Si is about 200 Å.

3.3 Energy Loss Calculations

The calculations will be done of the energy loss of He^+ and O^+ in going through the calculated projected range of Bi, i.e. 5.11 $\mu g/cm^2$. The He^+ energies that will be considered are 2.0, 1.0, and 0.5 MeV, but for the case of O^+, we consider only the 1.0 MeV case since these are the energies that will be used in our scattering experiments.

From Equation (2-13), the energy lost by the bombarding ion is the product of the stopping power and the projected range. For the evaluation of the stopping power, we will use the tables by Winterbon[5] for the case of 1.0 MeV O^+ since this is in the region where these tables are good. On the other hand, these tables are not good for He^+ and we have already direct experimental data by J.F. Ziegler and W.K. Chu[7] which we can use.

(a) Energy loss by helium ions: for He^+ penetrating Si targets we have the following values for the stopping power for different energies,

ENERGY,(MeV)	S,(eV/10^{15} atom/cm^2)
2.00	49.26
1.00	66.30
0.50	70.62

To change the dimensions of the stopping power from (eV/10^{15} atom/cm^2) to (MeV/$\mu g/cm^2$) we multiply by the conversion factor 21.5 x 10^{-6}.[8]

It should be noted that the energy lost by the ions depends on the angle ϕ between the direction of the incident beam and the normal to the target, and therefore will be different for different scattering angles in

the same energy region. For the sake of completeness we calculate the energy lost for each scattering angle at all energies considered. The values of the angle ϕ for different scattering angles will be shown in the next Chapter. Therefore, the actual amount of energy lost is $(SR_p/\cos\phi)$ since the actual distance the ions penetrate before reaching the Bi layer is $R_p/\cos\phi$. In the following table the energy lost to the nearest keV

ENERGY,(MeV)	SCATT. ANGLE,(DEGREES)	ϕ,(DEGREES)	ENERGY LOST,(keV)
2.00	160	-20.35	6
	140	- 0.35	5
	110	29.65	6
	90	49.65	8
1.00	160	-20.35	8
	140	- 0.35	7
	110	29.65	8
	90	49.65	11
0.50	160	-20.35	9
	140	- 0.35	8
	110	29.65	10
	90	49.65	13

(b) Energy loss by oxygen ions: neglecting the nuclear energy loss with compared to the electronic loss, the electronic stopping is given by[5]

$$S_e = \frac{\partial \varepsilon}{\partial \rho} = k \ \varepsilon^{1/2}$$

To convert this dimensionless energy loss to the usual dimensioned

quantities, we have

$$\frac{\partial E}{\partial R} = \frac{\rho}{\varepsilon} \frac{\partial \varepsilon}{\partial \rho} \quad (\text{keV}/\mu\text{g}/\text{cm}^2)$$

For 1.0 MeV O^+ incident on Si substrate, we have

$$\frac{\partial \varepsilon}{\partial \rho} = 0.1845\ (59.022)^{1/2}$$

$$= 1.4178$$

and therefore,

$$\frac{\partial E}{\partial R} = \frac{0.1400}{0.0590}\ (1.4178)$$

$$= 3.3620 \qquad \text{keV}/\mu\text{g}/\text{cm}^2$$

Again we calculate the actual energy loss for different scattering angles for 1.0 MeV O^+ (to the nearest keV)

ENERGY,(MeV)	SCATT.ANGLE, DEGREES)	ϕ,(DEGREES)	ENERGY LOST,(keV)
1.00	160	-20.35	18
	140	- 0.35	17
	110	29.65	20
	90	49.65	27

Subtracting these energy losses from the initial ions energy (E_o), gives us the actual energy at the scattering site (E_s) on which we make our calculations for the theoretical cross-section as discussed before.

3.4 Sources of Error

Now we discuss briefly the different sources of error that may occur during the implantation work and will certainly affect the scattering experiments.

(a) Uniformity of implantation: one of the main disadvantages of the self-supporting thin targets is the difficulty of obtaining a uniform target in this way. Sweeping the beam across the target accomplishes the uniformity of implantation.

Before starting the scattering experiments, a uniformity check test was done on the first Bi target. Considering a certain point in the implanted area as a centre of coordinates, we recorded the counts for the backscattered He^+ from different points taken at different locations in the (x,y) plane, the dimensions were in millimeters in both directions. The beam energy was 1.00 MeV, and the scattering angle was 160° for all the points. The target was mounted on a goniometer which allows movements in the horizontal and vertical directions. The counts from the center point (0,0) were repeated 8 times to get an average value for the counts for a fixed count rate on Hollis probe (100,000 Hollis counts were considered). The function and work of the Hollis probe will be described in the next Chapter. The average counts per 100,000 Hollis counts were 3708. The following table shows the counts at the different points and the % deviation from the average counts.

SCATT.POINT	COUNTS/100,000 HOLLIS COUNTS	% DEVIATION
(0,0)	3708	0.0
(1.5,0)	3662	-1.24
(3.0,0)	3708	0.0
(-1.5,0)	3880	4.64
(-3.0,0)	3690	-0.49
(0,1.0)	3768	1.62
(1.5,1.0)	3722	0.38
(-1.5,1.0)	3837	3.48
(0,-1.0)	3778	1.89
(1.5,-1.0)	3707	-0.03
(-1.5,-1.0)	3670	-1.02

From this table it is clear that most points are within $\sqrt{(\text{counts})}$ statistics which is about 1.6%, only 2 values lie outside twice the statistical accuracy which is acceptable. Therefore, we conclude that the uniformity of our targets is good.

(b) Neutral-atom component: in the 40 keV energy range, the Bi ions have a large cross-section for capturing an electron (from a residual gas atom) and become neutral atoms. These neutral atoms, if formed after the ion beam was deflected by the isotope separator analyzing magnet will hit the target without being counted by the beam integrator.

J. Pringle[9] did some experiments to check this neutral-atom component of the beam. He applied a positive retarding potential of 35 kv on the target while implanting 40 keV (Sb, Hf, Te) ions. In addition to the

5-keV range profile of the implanted ions, he noticed a tail due to the 40-keV neutral-atoms component. Extrapolating this tail, the neutral-atom component was found to vary from 0.5 to 1.0%.

However, during Pringle's work the pressure in the target chamber was about 6×10^{-6} torr, while in our implantations it was 1×10^{-6} and 2×10^{-6} torr. Therefore, since the neutralization probability/cm is directly proportional to the pressure, we can assume the neutral-component of the beam to be $\lesssim 0.5\%$ in our implantations.

(c) Current measurement: to measure the ion beam current, a Faraday-cup is mounted around the target. Precautions must be made to prevent the secondary electrons, which are generated by stopping the ion beam, from escaping through the entrance aperture of the Faraday-cup. Therefore, a negative bias of 120 V is applied on a grid plate outside the Faraday-cup to suppress the secondary electrons. Actually part of these secondary electrons escape from the Faraday-cup and this causes inaccuracy in the current measurement. On the isotope separator, the current measurements are accurate to about 1%.

(d) Sputtering: one more source of error in the implanted dose measurement is caused by sputtering especially when we implant high doses of the heavy ions (in the 10^{16} range). At the beginning of implantation, we have only sputtering of Si atoms, but as the implantation process continues, some of the Bi implanted ions will also be sputtered.

Now we make a rough estimate of the sputtering loss. The thickness of Si target removed due to sputtering is given by[10]

$$t = \frac{S.A}{\rho} \times D \times 0.0621 \quad \text{Å}$$

where t is the thickness sputtered away, S sputtering coefficient of Si by Bi (∿5 atoms/ion), A is the atomic weight of Si(=28), ρ is the Si density and D the implanted dose in $\frac{\mu A}{cm^2}$ min($1 \frac{\mu A}{cm^2}$ min $\equiv 4 \times 10^{14}$ ions/cm^2) substituting in the above equation gives (for 10^{16} ions/cm^2 dose)

$$t \simeq 20 \text{ Å}$$

Assuming that the range distribution has a Gaussian shape, we have the range straggling (ref.6, chap. 2), ΔR given by,

$$\Delta R = \frac{R_p}{2.5} = 80 \text{ Å}$$

Therefore from these estimates we can conclude that about 0.1% of the implanted ions have been sputtered away.

Actually, the range profile is skewed inside the material which will cause sputtered quantity less. Also we might have enhanced diffusion. Therefore as a rough estimate, we can assume a sputtering loss ∿0.5%

CHAPTER 4

EXPERIMENTAL SCATTERING MEASUREMENTS

The main scattering experiments are discussed in this Chapter. First the experimental arrangement is described. The experiments made for the energy calibration with the complete analysed results are also described. Also the ion current measurements by calibrating the Hollis probe against the Faraday-cup; this part will include the mechanism of the work of Hollis probe. The limitations on the count rates of the detectors and how to achieve these counts are given. Also, a description of the scattering from the Bi implanted layer and the method followed for the calculations of the required parameters. Finally, as we did in Chapter 3, we discuss the different sources of error and the experiments done to check them.

4.1 Experimental Arrangement

Figure 4.1 shows the experimental arrangement. The dashed lines indicate the incident and backscattered beams. The Hollis probe is labelled A, B is the Faraday-cup, C is the target and its holder, D is the target detector aperture, E is the arm connecting the detector aperture to the goniometer, F is the target detector, and S are the beam collimating slits.

Since the main purpose of this work is to check the angular and energy dependence of Rutherford law, as well as the absolute magnitude of

the scattering cross-section, therefore the first task was to develop suitable calibration techniques for accurate measurement of the scattering angles and energies, so as to study the backscattering at different angles and different energies.

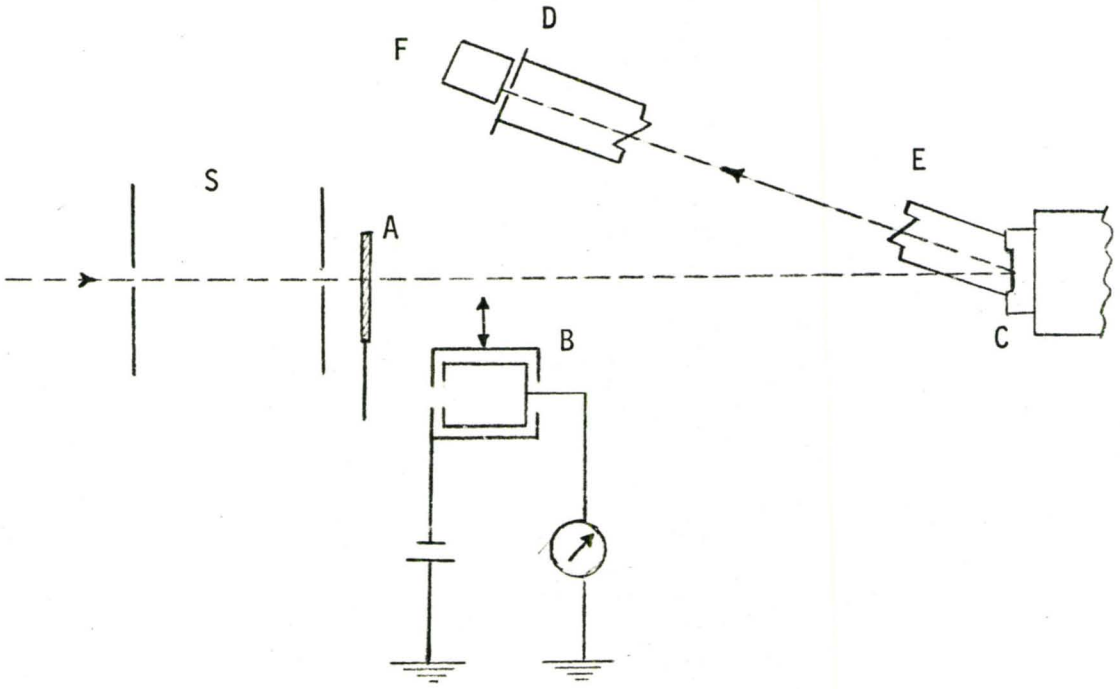

Figure 4.1 Experimental Arrangement

In the target chamber, the most accurate way to measure the scattering angles is to mount the detector on an arm rigidly vixed to the goniometer, so that the scattering angle is varied by rotating the top goniometer flange and we can determine this angle accurately.

The length of the arm on which we mounted the detector, i.e. the distance between the detector aperture and the target is 7.982 cm, and the aperture diameter is 2.25 mm. Therefore, the solid angle subtended by the detector at the target is

$$\omega = \frac{\pi}{4} \left(\frac{0.225}{7.982}\right)^2 = 0.000624 \text{ Sr.}$$

Before starting the scattering experiments, we made an accurate measurement of the angle between the detector arm and the beam direction. This was done by rotating the detector arm, and consequently the target (the detector was removed during this experiment) anti-clockwise from its initial position as shown in Fig. 4.1 (the beam is perpendicular to the target) until the beam passed through the center of the detector aperture and recorded the reading of the top flange. We obtained the following readings (we considered the readings on the right part of the flange to be negative):

READING	CURRENT CONDITION	REASON
-34.4°	- Goes to zero	Beam is intersected by the detector arm
-39.2°	- Starts to rise from zero	Beam starts to go through the aperture
-39.9°	- Reaches max. value	Beam is fully in the aperture
-40.8°	- Starts to fall down from max.	Beam starts to leave the aperture
-41.5°	- Goes to zero again	Beam is intersected by the other side of the detector arm

From these readings we find that at 39.55° the beam is at half-maximum in the rising part, and at 41.15° it is at half-maximum in the falling part, i.e. the aperture corresponds to 1.6° angular deviation. Therefore, the exact angle between the detector arm and the beam direction is $(39.55 + \frac{1.6}{2}) = 40.35°$

Before proceeding further we list the different scattering angles θ considered and the corresponding value of the angle ϕ between the incident

beam and the perpendicular to the surface. Figure 4.2 shows the different angles in our arrangement in a general position

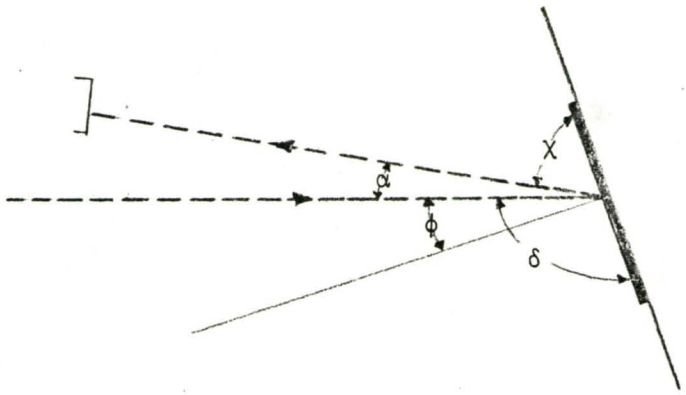

Figure 4.2 Different Angles Involved in the Scattering Experiments

The angles δ and χ between the incident beam and target surface, and the reflected beam and the target surface should always be greater than 30° so as to minimize multiple scattering. The scattering angle θ is $(180° - \alpha)$

θ	ϕ	δ
160°	-20.35°	110.35°
140°	- 0.35°	90.35°
110°	29.65°	60.35°
90°	49.65°	40.35°

The value of the angle χ is fixed (49.65°) and the minimum value of the angle δ is seen to be $\sim$40°, corresponding to the 90° scattering angle. The reason for choosing 160° as the largest scattering angle is that the Faraday-cup prevents further movements of the detector arm if we try to go to large scattering angles.

4.2 Energy Calibration Experiments

Since one of the main purposes of this work is to check the energy dependence of Rutherford Law, and the scattering cross-section is inversely proportional to the square of the energy. Therefore, to obtain good results we have to know the energy accurately.

The machine energy is read from the Differential Voltmeter on the main consol. Two different techniques have been used for checking the settings of the Differential voltmeter and to determine the exact energy corresponding to each setting.

The first technique involves the $Al^{27}(p,\alpha)$ nuclear reaction, where we make use of several sharp resonances of this reaction at accurately known energies. Therefore, the energy corresponding to a certain resonance will be the exact value of the energy for the Differential Voltmeter setting. In determining the resonance condition, we take the counts half-way in the rising part of the γ counts at that resonance. This calibration was done twice and the following table summarizes the results of these two runs.

RUN NO.	D.V. SETTING, (MeV)	RESONANCE ENERGY, (MeV)	$(\frac{D.V.}{E_{calib.}})$
1	2.009	1.095	1.0120
	1.406	1.3867	1.0139
	0.999	0.992	1.0065
2	1.407	1.3867	1.0146
	1.001	0.992	1.0091

From this table it is clear that the agreement between the two runs

is better than 0.3%.

In the second technique we use the 5.486 MeV alpha particles from an Am^{241} radioactive source for calibrating the linear Pulse Generator. Then, by comparing the backscattering spectrum of protons from gold targets, (two different targets were used, the first was a thin gold film deposited on a carbon substrate, and the second was a thick gold foil), with suitably chosen Pulse-Generator spectra, we can find the exact values of the energy corresponding to each Differential Voltmeter setting. Now we describe how the calculations procedure goes and then summarize the results from different runs in a tabular form.

First the Pulse Generator was set at 5.486 MeV, and the pulse peak was exactly in the same channel as Am^{241} alpha particles. To find the exact value of the energy corresponding to this Pulse Generator setting we have to subtract the amount of energy lost by the Am^{241} alphas in the detector dead gold layer which has a thickness of 700 Å, i.e. $\sim$135 $\mu g/cm^2$. This amount of energy lost was calculated by knowing the stopping power of gold targets for 5.486 MeV alpha particles[8], and this energy loss is 30 keV. Therefore, the exact energy for the Pulse Generator setting at 5.486 MeV is 5.456 MeV, (This correction is applied only to the first run, in the subsequent runs, we set the Pulse Generator at 5.456 MeV and by adjusting the normalizing potential we can make this pulse in the same channel as the 5.486 alphas, in this case no corrections will be made to the Pulse Generator settings). Since the Pulse Generator is linear, a correction factor of $\frac{5.456}{5.486}$, i.e. $\sim$0.995 must be multiplied by each setting to get the exact energy corresponding to that setting.

Now the backscattered spectrum of protons from gold at different Differential Voltmeter settings, i.e. different protons energies, was collected (scattering angles were 160° for the thin gold targets and 140° for the thick target). Also pulses of different energies from the Pulse Generator were collected. From the Pulse Generator settings and the collected backscattered spectra we can find the energy corresponding to the gold peak (thin target), and the mid-point of the gold edge (thick target) by determining the channel in which this peak (or edge) lies and calculating the energy corresponding to this channel from the Pulse Generator. Each calculated energy is now multiplied by the correction factor mentioned before to account for the Pulse Generator calibration (for the first run only in this work). Then to these corrected energies we add the amount of energy lost by protons in traversing the thin (135 $\mu g/cm^2$) dead gold layer on the detector surface[8], and thus obtain the proton energy just after scattering from gold. Since the proton loses 0.0195 of its initial energy in scattering at 160° from gold, (and 0.0178 of its initial energy at 140°), we can determine, therefore, the initial proton energy before scattering, which should be the exact energy corresponding to the specific Differential Voltmeter setting.

The following table summarizes the results for the different runs after performing all the required calculations

RUN NO.	GOLD TARGET USED	D.V.,(MeV)	$E_{calib.}$,(MeV)	$(\frac{D.V.}{E_{calib.}})$
1	Thin	2.04	1.9889	1.0257
		1.406	1.3865	1.0141

RUN NO.	GOLD TARGET USED	D.V.,(MeV)	$E_{calib.}$,(MeV)	$(\frac{D.V.}{E_{calib.}})$ (cont'd)
		1.00	0.9835	1.0168
		0.51	0.5058	1.0083
2	Thick	2.04	1.9805	1.0301
		1.406	1.3806	1.0184
		1.00	0.9765	1.0241
		0.51	0.5028	1.0143
3	Thick	2.04	1.9732	1.0338
4	Thick	2.04	1.9772	1.0318
		1.00	0.9806	1.0198
		0.51	0.5056	1.0087

From this table, it is clear that the energy calibration using thick targets are reproducible to better than 0.4%. But these values are about 1% less than that for the thin target.

Comparing these values of calculated energies to those given by the $Al^{27}(p,\alpha)$ calibration, we notice that the thin target energies are about 1% higher and the thick target energies are about 2% higher.

Actually the calibration using the $Al^{27}(p,\alpha)$ nuclear reaction should be the best since the energies for the different resonance are accurately known, and the method itself is straightforward and needs no calculations. But in our calculations for the energy dependence and the total Rutherford scattering cross-section, we will use the values of energies calibrated by the thin film target as intermediate values between the other two cases.

4.3 Ion Current Measurements

The ion current is measured by the use of a Faraday-cup which determines the amount of charge corresponding to the incident ion beam. Since it is not possible to use the Faraday-cup and the target simultaneously (the Faraday-cup completely intersects the beam and prevents it from hitting the target), therefore, the Faraday-cup is made removable as shown in Fig. 4.1 and a coupling between the Faraday-cup and the target is used. This coupling is called the Hollis probe which is a thin gold layer of thickness about 700 Å deposited on a aluminium foil, the side of the foil facing the beam is cut at 45° inclination and the scattering from this probe is taken at a scattering angle 90°, as shown in Fig. 4.3 in which A is the Hollis probe, G the detector, H the detector aperture, and S are the beam collimating slits.

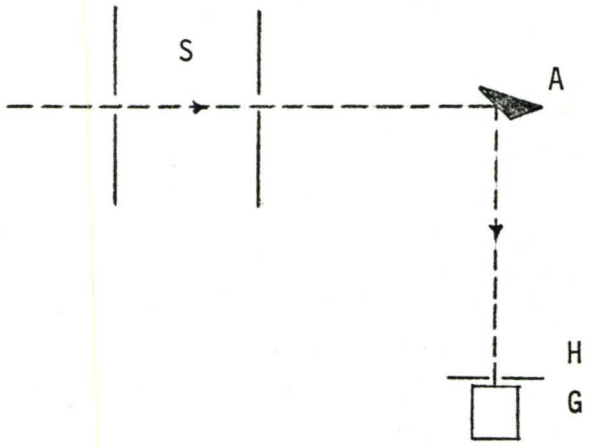

The Hollis probe oscillates continuously across the beam during both the Faraday-cup calibration and the scattering experiments. Therefore by continuously intersecting the beam at a constant speed, by using an external

motor, the counts for the 90° scatterings are detected by the detector G in the bottom of the target chamber.

An aperture (H) of 1-3 mm diameter is put over the Hollis probe detector to limit the total count rate with the probe in the static position (i.e. the Hollis probe completely intersecting the beam) to less than 3000 counts/sec in order to avoid undue noise and dead-time losses. A similar counting restriction (i.e. <3000/sec) applies to the main detector, and this is partly accomplished by the apertures on the detectors and partly by adjusting the magnitude of the ion current.

For ion current measurements, the Hollis probe is calibrated against the Faraday-cup to find the number of Hollis probe counts for a certain amount of charge collected by the Faraday-cup, then we find the number of the counts from backscattering of the target corresponding to a certain number of Hollis probe counts. From these two measurements, we can determine the number of incident ions on the target, and hence the number of backscattered ions per microcoulomb of charge collected by the Faraday-cup, i.e. 6.23×10^{12} ions incident on the target, these calculations will be done in the next Chapter.

The counts from the Hollis probe were determined by the settings of the window of the single channel analyser. Two different ways of these settings were made, the first we considered only the counts due to the gold peak of the spectrum, but to get better statistical accuracy, the window settings(lower disc.) was made wider to allow for a part of the aluminium spectrum to be counted.

The charge collected by the Faraday-cup is determined by the Beam Current Integrator. The 10-turn Trip Level control was always set to the value 100 (full-scale setting), then the number of times (clicks) the integration circuit must recycle to provide the necessary integration period, this was taken between 1 and 3 clicks. Now for determining the amount of charge (Q) collected for a full-scale (100) Trip Level setting

$$Q = 100 \times \text{Electrometer Scale} \times \text{No. of Clicks}$$

where Q is in Coulombs. A negative potential of 300 V is applied to the Faraday-cup for secondary electrons suppression.

4.4 Backscattered Spectrum

Since the Bi ions are implanted in low Z substrate (Si), therefore the backscattered spectrum is composed of two distinct regions, a continuous low energy part with a sharp edge due to scattering from Si and a peak at much higher energy due to scattering from Bi.

In this work we are studying the backscattering from Bi,and therefore a window width is set to accept only the counts from the Bi scattering (the peak in the spectrum). In setting the window levels, it is important that the lower edge of the window does not include the part of the spectrum from Si (since Si edge is not vertical and there is a tail extended to higher energies) in the low energy side of the peak especially when the incident ion energy is 0.5 MeV. Also we must be sure that the window always includes the Bi peak for all the scattering angles since the Si edge moves towards

the higher energy side in a larger rate than the Bi peak for smaller scattering angles (90°), so the separation between the Bi peak and the Si edge becomes smaller and the Bi window might include some of the Si counts if not set properly to account for this factor.

In the scattering experiments, we record the counts from Bi scattering corresponding to a certain amount of counts on Hollis probe. The number of counts on Hollis probe is chosen so that the counts from both the Hollis probe and the Bi target are large enough to give better statistical accuracy.

4.5 Calculations Procedure

In this section we discuss how to use the data taken from the experimental work and apply it to check the validity of the Rutherford law as was shown in Chapter 2.

The number of backscattered ions (I) in Equations (2-12), (2-15) and (2-16) will be those corresponding to a number of incident ions equivalent to 1 μc on the Faraday-cup, i.e. I_o in Equation (2-12) is 6.23×10^{12} ions.

In our experiments, we have the number of backscattered ions (I_1) for a certain number of counts on the Hollis probe (I_2). From the Hollis probe calibration, we get I_3 counts corresponding to an amount of charge q μc on the Faraday-cup. Therefore the number of backscattered ions (I) per 1 μc is given by

$$I = \frac{I_1}{I_2} \frac{I_3}{q} \qquad (\text{counts}/\mu c)$$

The detailed calculations and results will only be given in its final form in the tables of Chapter 5. We will follow exactly the procedure explained in details in Chapter 2.

4.6 Sources of Error

As we did in the previous Chapter, we now discuss the different sources of error during the scattering experiments.

(a) Energy of the Machine: as we mentioned in section 4.2, it is very important to know the energy of the incident beam accurately. But from the energy calibration of the machine and due to our choice of the thin gold film calibration, we would expect an error of about ±1% in the energy used in the calculations.

(b) Hollis Probe: as mentioned in section 4,3, the Hollis probe is used as a coupling between the Faraday-cup and the target for ion current measurements. Therefore, the counts given by the Hollis probe should be accurate. In the first calibrations we used the counts from gold scattering only (gold peak), but this requires long counting time to obtain good statistical accuracy. We changed this scheme and made the window wider to include part of the aluminium spectrum which gives good statistical accuracy in short time. But as the beam continues hitting the Hollis probe, a carbon spot is formed on the gold film and this causes a change in the counts obtained. Therefore we often moved the Hollis probe to allow the beam to hit a new spot. Another factor is that the gold film, which is about 700 Å, might not be uniformly deposited on the aluminium substrate and this will cause deviations in the counts of the beam deviates a short distance from

its actual path or when we move the foil to a new spot.

Another problem we noticed is that the zero setting of the Electrometer microammeter needed to be adjusted at frequent periods during the run. This, if not adjusted, will cause an error in the amount of charge collected. We expect that this might require readjustment during the same count, which is impossible, and therefore may contribute some error in the calibration.

The observed Hollis probe counts were reproducible to about ±2% for the 2 MeV ions. But for the 0.5 MeV case, it sometimes becomes more than 3%. To reduce these fluctuations, we made the Hollis probe calibration before and after each scattering point and took the average of these different calibrations as the correct counts for the Hollis probe.

We tried to replace this technique for ion current measurements by building a copper screen cage around the target, and therefore we can replace it instead of the whole system of the Hollis probe and the Faraday-cup. This screen is used to suppress the secondary electrons which resulted from the stopping of the ions by the target (a negative potential of 300 V was applied on the screen). But when this arrangement was checked against the usual Faraday-cup system using He^+ at energy 2 MeV, the region in which the Hollis probe works properly, we found that the Hollis probe counts were always less for the new proposed arrangement (target-Screen) by about 5%. This difference is caused by the fact that, inspite of the negative potential on the screen, some of the secondary electrons escape through the openings of the screen.

Therefore due to these problems in the Hollis probe, we expect an

experimental error of about ±2%.

(c) Charge Exchange: after the accelerated ions leave the magnetic field they are composed of singly charged ions. But there is a certain probability that some of these ions lose (or capture) an electron and become double charged (or neutral). In the MeV energy range, the cross-section of the ion to lose an electron is much higher than that to capture an electron. The probability that an ion will lose its single charge state is given by

$$Pr(+ +) = (\sigma_{loss} - \sigma_{capt.}) \times N_{cc} \times \ell$$

where σ_{loss} and $\sigma_{capt.}$ are the cross-section to lose and to capture an electron respectively, N_{cc} is the number of gas molecules per c.c., and ℓ is the path length after the magnet. Since N_{cc} is proportional to the pressure of the system, therefore the operating pressure greatly affects this phenomena.

The values of σ_{loss} range from 10^{-17} to 10^{-16} cm^2/ion, and the highest value observed for oxygen is $\sim 3 \times 10^{-16}$. Generally σ_{loss} is higher for heavier particles.

We did an experiment for testing the pressure effect on Faraday-cup/Hollis probe calibration using He^+ and O^+. The following table summarizes the experiment done. The pressure is recorded in the target chamber.

From this experiment, it is clear that, unless the recorded vacuum in the target chamber is better than 2×10^{-6} torr, we can expect a significant error due to the charge exchange phenomena. Under our operating conditions ($\lesssim 2 \times 10^{-6}$) this error is estimated to be $\lesssim 1\%$.

Ions	Pressure,(Torr)	Hollis Counts/μc
He^+	5.8×10^{-5}	1588
	5.1×10^{-5}	1687
	4.8×10^{-5}	1729
	4.0×10^{-6}	1879
	3.0×10^{-6}	1837
	2.8×10^{-6}	1887
	2.4×10^{-6}	1902
	2.1×10^{-6}	1833
	1.8×10^{-6}	1891
	1.7×10^{-6}	1927
	1.6×10^{-6}	1909
	1.5×10^{-6}	1886
O^+	2.2×10^{-5}	219560
	1.2×10^{-6}	240433

(d) Target-Detector Geometry: in the evaluation of the absolute scattering cross-section, we need to know the exact value of the solid angle subtended by the detector at the target. This means the exact measure of the detector aperture diameter (this was measured using a drill of known diameter) and length of the detector arm (using a pencil-shape pointer and measuring its length by a vernier caliber). In this work, we expect an error of about ±0.5% in each of these measurements.

CHAPTER 5

RESULTS AND DISCUSSIONS

The complete analysed final results of the scattering experiments are put in the form of tables. The analysis of the experimental data follows exactly the theoretical framework in Chapter 2, and making use of the calculations made in Chapter 3 for the energy lost by the ions in penetrating the Si substrate. These tables are followed with a discussion of the results we obtained and the final conclusion.

5.1 Results

The results are put in 3 tables, Table I for angular dependence, Table II for the energy dependence, and Table III for the absolute scattering cross-section (experimentally and theoretically). Tables marked by the letter "A" are for He^+ scattering from Bi, and those marked by the letter "B" are for O^+ scattering from Bi too. In Tables I and II, the last column is the normalized counts (for angular dependence and energy dependence respectively) per Bi implanted ion. This column is done as a check for the reproducibility of the results using different targets.

For these calculations, we used these values for the required parameters:

(a) He^+/Bi scattering:

$M_1 = 4$, $M_2 = 209$

$Z_1 = 2$, $Z_2 = 83$

(b) O^+/Bi scattering:

$M_1 = 16$, $M_2 = 209$

$Z_1 = 8$, $Z_2 = 83$

It should be noted that the scattering angles listed in the tables are the laboratory scattering angles. It should be transformed to the C.M. angles using Equation (2-1) before being used in the calculations.

Table I(A)

Angular Dependence, He^{+}/Bi Scattering

Run & Target No.	D.V., MeV	Scatt. Angle, Degrees	Backscattered Counts per H.P. Counts	Counts/ μc	Norm. for Ang. Dep	Norm. for Bi Density ($x10^{-15}$)
1,1	2.04	160	6616/10,000 on H.P.	78.93	72.35	36.75
		140	7490/10,000 on H.P.	89.36	72.40	36.77
		110	14869/10,000 on H.P.	177.4	72.20	36.67
		90	42706/10,000 on H.P.	[509.5]*	[85.62]*	[43.49]*
	1.04	160	5367/10,000 on H.P.	295.1	270.5	137.4
		140	5846/10,000 on H.P.	321.4	260.4	132.3
		110	11577/10,000 on H.P.	636.5	259.1	131.6
		90	28598/10,000 on H.P.	1572	264.2	134.2
2,2	2.04	160	8282/100,000 on H.P.	[380.5]*	[348.0]*	[34.4]*
		140	9598/100,000 on H.P.	443.1	360.0	35.5
		110	14997/80,000 on H.P.	886.6	360.8	35.6
		90	18304/40,000 on H.P.	2180	366.4	36.2
	0.51	160	5956/40,000 on H.P.	6859	6288	620.9
		140	6590/40,000 on H.P.	7483	6062	598.6
		110	6715/20,000 on H.P.	15186	6181	610.3
		90	16321/20,000 on H.P.	37529	6307	622.8
3,2	2.04	160	16727/80,000 on H.P.	393.8	361.0	35.65
		140	19169/80,000 on H.P.	450.8	366.0	36.07
		110	19004/40,000 on H.P.	896.2	364.7	36.02
		90	23523/20,000 on H.P.	2224.	373.7	36.90
4,2	0.51	160	14879/80,000 on H.P.	[6351]*	[5822]*	[574.9]*
		140	17055/80,000 on H.P.	7493	6071	599.5
		110	17287/40,000 on H.P.	14959	6088	601.2
		90	83518/40,000 on H.P.	37821	6356	627.7

*Anomalous counts

Table I(B)

Angular Dependence, O^+/Bi Scattering

Run & Target No.	D.V., MeV	Scatt. Angle, Degrees	Backscattered Counts per H.P. Counts	Counts/ μc	Norm. for Ang. Dep.	Norm. for Bi Density ($\times 10^{-15}$)
1,2	1.00	160	11330/100,000 on H.P.	2700	2775	274.0
		140	12779/100,000 on H.P.	3042	2775	274.0
		110	20096/80,000 on H.P.	6047	2757	272.3
		90	24926/40,000 on H.P.	15192	2859	282.4

Table II(A)

Energy Dependence, He^+/Bi Scattering

Run & Target No.	Scatt. Angle, Degrees	D.V., MeV	E_o MeV	E_s MeV	Counts/ μc	Norm. for Energy Dept.	Norm. for Bi Density ($x10^{-15}$)
1,1	160	2.04	1.9889	1.9832	98.93	310.4	157.7
3,2		2.04	1.9889	1.9832	393.8	1549	152.9
1,1		1.04	1.0222	1.0144	295.1	303.7	154.2
2,2		0.51	0.5058	0.4969	6859	1693	167.2
1,1	140	2.04	1.9889	1.9835	89.36	351.6	178.6
2,2		2.04	1.9889	1.9835	443.1	1743	172.2
3,2		2.04	1.9889	1.9835	450.8	1774	175.2
1,1		1.04	1.0222	1.0149	321.4	331.1	168.2
2,2		0.51	0.5058	0.4974	7483	1851	182.8
4,2		0.51	0.5058	0.4974	7493	1854	183.1
1,1	110	2.04	1.9889	1.9827	177.4	697.3	354.2
2,2		2.04	1.9889	1.9827	886.6	3485	344.2
3,2		2.04	1.9889	1.9827	896.2	3523	347.9
1,1		1.04	1.0222	1.0138	636.5	654.2	332.3
2,2		0.51	0.5058	0.4962	15186	3738	369.1
4,2		0.51	0.5058	0.4962	14959	3682	363.6
2,2	90	2.04	1.9889	1.9806	2180	8552	844.5
3,2		2.04	1.9889	1.9806	2224	8723	861.4
1.1		1.04	1.0222	1.0110	1572	1607	816.3
2,2		0.51	0.5058	0.4928	37529	9115	900.1
4,2		0.51	0.5058	0.4928	37821	9186	907.1

Table III(A)

Absolute Cross-Section per Steradian, He^+/Bi Scattering

Run & Target No.	D.V., Mev	E_o MeV	Scatt. Angle, Degrees	E_s MeV	Exp. cross-section $(x10^{-24})cm^2/sr.$	Theor. cross-section $(x10^{-24})cm^2/sr.$	% Deviation $[\frac{(Exp.-Theor.)}{Theor.} \times 100]$
1,1	2.04	1.9889	160	1.9832	10.03	9.787	2.43
			140	1.9835	12.02	11.83	2.52
			110	1.9827	20.41	19.98	2.15
	1.04	1.0222	160	1.0144	37.49	37.40	0.222
			140	1.0149	43.26	44.80	-3.43
			110	1.0138	73.25	76.41	-4.14
			90	1.0110	133.02	136.8	-2.78
2,2	2.04	1.9889	140	1.9835	11.73	11.83	0.026
			110	1.9827	19.83	19.98	-0.73
			90	1.9806	35.86	35.65	0.575
	0.51	0.5058	160	0.4969	169.4	155.9	8.65
			140	0.4974	195.8	186.5	4.97
			110	0.4962	339.7	316.1	6.47
			90	0.4928	617.2	575.8	7.20
3,2	2.04	1.9889	160	1.9832	9.70	9.787	-0.879
			140	1.9835	11.80	11.83	0.571
			110	1.9827	20.05	19.98	0.345
			90	1.9806	36.41	35.65	2.12
4,2	0.51	0.5058	140	0.4974	196.0	186.5	5.12
			110	0.4962	334.6	316.1	4.88
			90	0.4928	622.0	575.8	8.04

Table III(B)

Absolute Cross-Section per Steradian, $0^{+}/Bi$ Scattering

Run & Target No.	D.V., MeV	E_o MeV	Scatt. Angle, Degrees	E_s MeV	Exp. cross-section $(x10^{-24})cm^2/sr.$	Theor. cross-section $(x10^{-24})cm^2/sr.$	% Deviation $[\frac{(Exp.-Theor.)}{Theor.} \times 100]$
1,2	1.00	0.9835	160	0.9652	742.7	693.9	7.02
			140	0.9664	873.1	813.9	7.27
			110	0.9638	1411	1331	6.03
			90	0.9570	2506	2311	8.42

5.2 Discussions

Here we discuss each item we have checked its validity alone, but first we discuss the reproducibility of the experimental results we obtained.

(a) Reproducibility: the extent to which our results are reproducible can be shown in Table I. The only two energies for which we repeated the runs are the 2 MeV and 0.5 MeV, with different targets for the first and the same target for the second. Also we repeated some counts in the last 3 runs for He^+ and for the O^+ run. From the counts we obtained (the 5th column of Table I, and the repeated runs), we can see that the counts are reproducible to $\pm 2\%$, except for the anomalous counts observed (counts in square brackets in all the tables). These counts will be put in Table I only and excluded for the other tables.

(b) Angular dependence: As we see from the last two columns in Table I(A), the angular dependence deviates from that predicted by Rutherford law by about twice the reproducibility limit ($\pm 2\%$). The same percentage of deviation from the theoretical predictions are also observed for the case of O^+ (Table I(B)).

(c) Energy dependence: From the last two columns in Table II(A), the energy dependence for the 2 MeV and 1 MeV deviates by twice the reproducibility limit and about 2.5 times the reproducibility for the 0.5 MeV case.

(d) Absolute cross-section: In the last column of Tables III(A) & (B), we evaluate the percentage deviation between the experimentally

determined cross-section and the theoretically calculated cross-section. As shown in this column, the average deviation is about 2%. But for the 0.5 MeV He^+ and 1 MeV O^+ cases, the experimental cross-section is much higher than the theoretical, both these cases are the largest impact parameters collisions where we expect deviation from Rutherford law. However, this trend is opposite to what would be expected due to the effect of screening of atomic electrons. The reason for this opposite condition might be due to multiple scattering with Bi atoms, but the effect of multiple scattering should not be so high.

It should be noted that these validity estimates are only based on the experimental data we obtained and no adjustment is done to account for the different sources of error discussed in the previous chapters.

5.3 Conclusion

We examined the validity of Rutherford Law by studying the scattering of He^+ and O^+ from Bi, both the angular and energy dependence were checked and the results obtained do not vary much from the reproducibility of the different runs. The magnitude of the absolute cross-section was compared with the theoretical value. The experimental values lie within the reproducibility limits (±2%). This made us conclude that the different sources of error have opposite effects on the overall counts. The 0.5 MeV He^+ and 1.0 MeV O^+ cases, the largest impact parameters studied, showed higher values of the absolute cross-section than the theoretical value (about 5% higher) which is contradicting with what would be expected

from the screening effect of orbital electrons. More work is required to find the reason for this contradiction.

The targets used were made by implanted 40 kV Bi ions in Si substrate and therefore we obtained a uniform thin film of Bi for the scattering experiments.

References

(1) Rutherford, E., Phil. Mag., 21, 669 (1911).

(2) H.H. Anderson, J. Bottiger, and H. Knudsen, Phys. Rev., A7, 154 (1973).

(3) J.F. Ziegler and J.E.E. Baglin, Int. Conf. on Ion Beam Surface Layer Analysis, York Town Heights, New York, (1973).

(4) Evans, The Atomic Nucleus, Appendix B, p.828, McGraw-Hill (1955).

(5) K.B. Winterbon, AECL-3194, Nov. (1968).

(6) J. Mayer, L. Erikson, J. Davies, Ion Implantation in Semiconductors, p.28, Academic Press (1970).

(7) J.F. Ziegler, W.K. Chu, IBM Research, RC 4288, March 29, (1973).

(8) Ward Whaling, The Energy Loss of Charged Particles in Matter, Handbuch der Physik, Bd. XXXIV.

(9) J. Pringle, Private Communications, (1973).

(10) R. Kelly, Canadian Journal of Physics, 46, 473 (1968).

A MONTE-CARLO TECHNIQUE FOR THE CALCULATION OF keV ION BACK-SCATTERING FROM METAL SURFACES

by

Said Agamy

PART B: ON-CAMPUS PROJECT*

A project report submitted in partial fulfillment of the requirements

for the degree of

Master of Engineering

Department of Engineering Physics

McMaster University

Hamilton, Ontario

April, 1973

*One of two project reports: The other part is designated PART A: MCMASTER INDUSTRIAL PROJECT

Supervisor: Dr. J.E. Robinson

Number of pages: 58

ACKNOWLEDGMENT

The author wishes to express his deep thanks and gratitude to Dr. J.E. Robinson, Department of Engineering Physics, McMaster University, Hamilton, Ontario, Canada for his supervision, unfailing help, discussions and encouragement during the course of this work.

ABSTRACT

As an introduction to a larger study of ion bombardment phenomena on metal surfaces, we apply the Monte-carlo technique to calculate the range distribution and back-scattering of keV ions from metal surfaces. Lindhard theory is used to calculate both the ion-metal atom scattering and the electron stopping power. The program can be used over a wide range of reduced energies ($.1 < \varepsilon < 30$) limited only by the validity of the Lindhard theory. A sample calculation of hydrogen scattering from aluminum is presented.

CONTENTS

CHAPTER 1

Introduction and Review

1.1 Introduction

In this report, a Monte-Carlo program is described and sample problem demonstrated for the calculation of projected range distributions and back-scattering of light Kev ions incident on amorphous solids. This particular report is the beginning of a larger study of ion bombardment phenomena on metal surfaces.

The Monte-Carlo method has been chosen to calculate range distributions and back-scattering since,

(1) the Thomas-Fermi cross section can be conveniently used for the reduced energy range $0.1 < \varepsilon < 30$,

(2) electron stopping can be treated for $v < v_0$ using the Linhard model,

(3) the "surface correction" for the range distribution is automatically incorporated into the calculation, and

(4) both the angular and the energy distributions of the scattered particles can be determined.

The main disadvantage of this method is that a large number of particles must be followed to obtain sufficient accuracy.

After a brief review of the current work on back-scattering on Chapter 2, we discuss the particle interactions and the energy loss mechanisms. In Chapter 3, the detailed calculations of the ions back-scattering will be established using the Thomas-Fermi potential. In Chapter 4, we will put the

computer results of the calculations and the conclusion. The computer programs that were used will be listed in the appendix.

1.2 Review:

Most of the work done on ion bombardment of solids was devoted to the range calculations, the spatial distribution of deposited energy, and the sputtering calculations. Among the Monte Carlo calculations for the ranges of energetic atoms in solids O.S. Oen et al. (1963) used the Monte Carlo technique to find the ranges using Bohr potential:

$$V(r) = \frac{E_B}{2} \frac{\exp(-r/a_B)}{r/a_B}$$

where

$$E_B = 2Z_1Z_2 e^2/a_B$$

and the screening length is given by

$$a_B = k\, a_H/(Z_1^{2/3} + Z_2^{2/3})^{1/2}$$

where $a_H \equiv$ the first Bohr potential (0.529°A). In the above Z_1 and Z_2 are the atomic numbers of the primary and struck atoms, respectively. The factor k which was introduced as an adjustable parameter; this was taken as unity. Also O.S. Oen et al. presented in (1964), Monte Carlo calculations using the Thomas-Fermi potential:

$$V_{TF}(r) = (Z_1Z_2e^2/r)\, \phi_{TF}\, (r/a_F)$$

where $\phi_{TF}(x)$ is the Thomas-Fermi screening function, the screening length a_F was represented by

$$a_F = 0.8853\ a_H/(Z_1^{1/2} + Z_2^{1/2})^{2/3}$$

They employed the Sommerfield approximation to the Thomas-Fermi screening function:

$$\phi_{TF}(x) = [1 + (x/\alpha_1)^{\alpha_2}]^{-\alpha_3}$$

where $\alpha_1 = 12^{2/3}$, $\alpha_2 = 0.8034$, and $\alpha_3 = 3.734$ are the values of constants determined by March. In this paper they compared their calculations for both the Bohr and Thomas-Fermi potentials and found that the experimental results lie between the calculated results of the two potentials, but they found that the thomas-Fermi potential gives a somewhat better over-all description of the true interatomic potential.

G.M. McCracken and N.J. Freeman (1969) derived an expression for the back-scattering of Kev hydrogen ions in solids by assuming that the incident ions are scattered in a single wide-angle collision and that the energy loss in the solid is due only to interaction with electrons. They assumed also that Rutherford scattering applies to the collision of interest and used the differential scattering cross-section

$$\sigma(E,\theta)\ d\omega = \frac{1}{16}\left(\frac{Z_1^2 Z_2^2\ e^4}{E^2}\right) \operatorname{cosec}^4\left(\frac{\theta}{2}\right) d\omega$$

where E is the ion energy and θ the scattering angle. They rendered the deviations from experimental results due to the fact that the incident ion may

undergo multiple scatterings rather than a single scattering event.

A. Van Wijngaarden et al. (1971), studied the energy spectra of Kev back-scattered protons. The model used to derive the theoretical energy distribution of projectiles back-scattered from an uniform film was: each back-scattered projectile is scattered at an angle θ_L in a single hard nuclear collision. During its travel from the film surface to the scattering site and back, the projectile gradually loses energy in many electronic collisions and in small-angle nuclear collisions, but its direction of motion is not significantly affected. Also, there was a difference between theory and experiment on the low-energy side, and they referred this difference, especially for thick films to multiple scattering in nuclear collisions and from non-uniformities in film thickness.

The moments method using an Edgeworth expansion was discussed by J. Bottiger et al. (1971), where they used the penetration profile F(x) as a function of depth x in an infinite target to calculate the reflection coefficient R which was defined as the fraction of the beam that has a negative penetration depth, i.e.

$$R = \int_{-\infty}^{0} F(x)\, dx$$

They also included connections to the calculated values due to electronic stopping and surface effects. They obtained satisfactory agreement between measurements and calculations.

A Monte-Carlo technique was used by K. Güttner et al. (1972) for calculations of the back-scattering of high-energy heavy ions from metal surfaces. Their fundamental method consisted of following single particle histories in metal

films of known thickness. The atoms in the film were assumed to be in no regular order, an assumption being satisfactorily fulfilled by polycrystalline foils. Each ion traverses several layers without any reflection but with continuous energy losses by excitation and ionization of the atomic electrons. At the end of each of these paths the particle suffers a deflection interacting with only an film atom at the moment. The length of the paths and the scattering angles were selected by random numbers applying mere classical formulaes. The potential used was:

$$V(r) = \frac{Z_1 Z_2 e^2}{r} \exp(-r/a)$$

where the screening parameter a was given by Bohr as

$$a = a_H/(Z_1^{2/3} + Z_2^{2/3})^{1/2} \quad , \quad a_H = 0.529 \ ^{\circ}A$$

on the assumed potential they fitted a screened Coulomb potential,

$$V(r) = E_c \left(\frac{a_c}{r} - 1\right)$$

where E_c and a_c are constants.

Satisfactory agreement with known experiments was obtained.

CHAPTER 2

Interactions Between Atoms

2.1 Introduction:

We are considering in this work two types of interactions between the incident particle and the target atom. The first one is the elastic scattering collisions with atomic nuclei and all the particle deflections from its original path are considered to be due to this interaction process. The second is the inelastic interaction, or inelastic energy loss due to excitation of atomic electrons, this is a continuous interaction process and predominates at high particle energies. Due to these two interaction processes the projectile will eventually lose its energy and suffer deflections from its path. We will consider the elastic collisions in more detail and for the electronic energy loss will make use of the work of Linhard and Scharff (1961).

2.2 Elastic Collisions:

We assume that collisions between the incident particle and the lattice atoms can be treated classically by isolated two body events, then our problem will be the complete determination of the trajectory of the projectile when acted upon by the interatomic force between the projectile and target atom with which it is in collision. The trajectory of the projectile may be depicted as in figure 2.1. In the absence of any force of interaction F(r) between the partners (primary and struck or target atom) the primary would pass within a minimum distance p, known as the impact parameter, from the struck atom and continue undeflected.

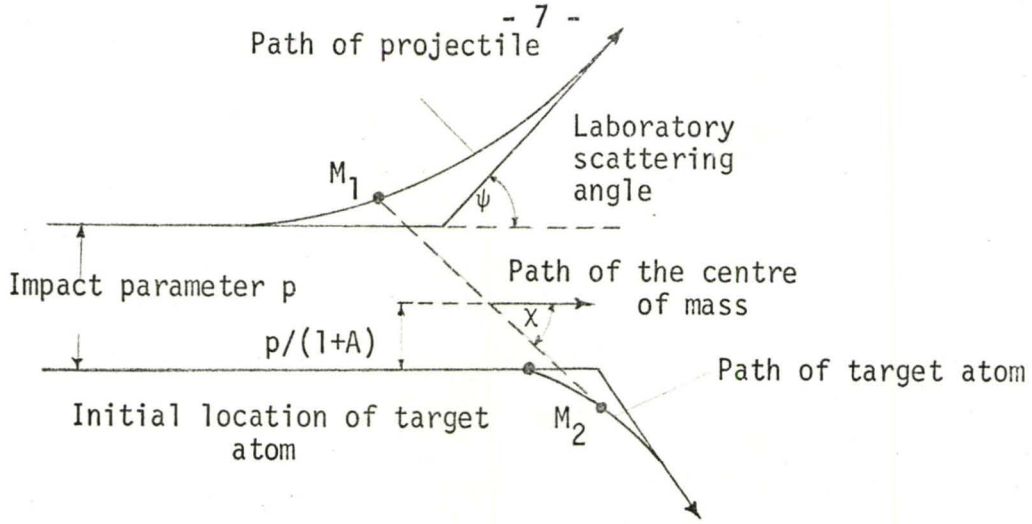

Fig. 2.1: The scattering of a projectile by a target atom

However, because of the force F(r), where r is the distance between the partners), the primary is deflected through an angle ψ measured in the laboratory system, and the struck atom moves away at some angle χ to the original direction of the primary. Energy is patently transferred from the primary to the struck atom and the amount of energy transferred or remaining with each collision partner can be calculated.

2.2.1 Energy Transferred and Projectile Deflection Angles:

In this section we are going to put the equations governing the interaction process, the details of the derivation can be found in "Ion bombardment of solids, Carter & Colligon". Figure 2.2 shows the different velocities in both laboratory and centre of mass systems.

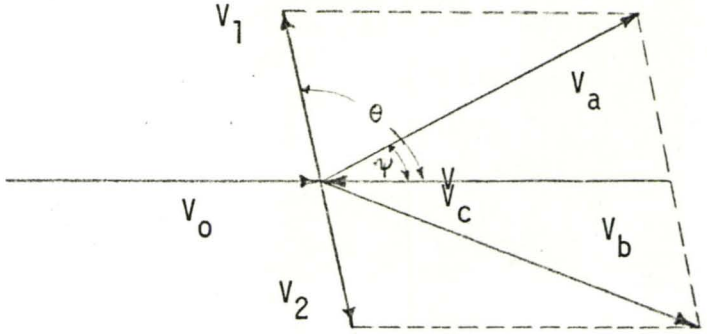

Fig. 2.2: Velocity vector diagram in the centre of mass system

obtain

$$V_a^2 = v_o^2 \frac{[1 + A^2 + 2A \cos\theta]}{(1 + A)^2} \qquad (2.1\ a)$$

$$V_b^2 = \left[\frac{2\ v_o \sin \theta/2}{1 + A}\right]^2 \qquad (2.1\ b)$$

where $A = M_2/M_1$

It is evident that the relation between the scattering angle ψ is the lab. system and θ in the C.M. system is

$$\tan \psi = \frac{V_1 \sin \theta}{V_c + V_1 \cos\theta} = \frac{A \sin \theta}{1 + A \cos \theta} \qquad (2.2\ a)$$

and $\chi = \frac{\pi}{2} - \frac{\theta}{2}$ for the struck atom in the lab. system (2.2 b)

The energy lost by the primary in the collision, T, is equal to that gained by the struck atom, and from equation (2.1 b) we can get,

$$T = \frac{2\ M_2\ v_o^2 \sin^2 \theta/2}{(1 + A)^2} \qquad (2.3\ a)$$

or in terms of the primary energy E_o,

$$T = (1 - \alpha)\ E_o \sin^2 \theta/2 \qquad (2.3\ b)$$

where

$$\alpha = \left[\frac{A - 1}{A + 1}\right]^2$$

In a head-on collision between partners ($\chi = 180^\circ$) i.e. the struck atom moves parallel to the original direction of motion, $\theta = -180^\circ$ and the motion

of the primary is reversed. The maximum energy transfer in such a collision is thus

$$T_m = (1 - \alpha)\, E_o = \frac{4\, M_1 M_2}{(M_1 + M_2)^2}\, E_o \qquad (2.4\ a)$$

and therefore

$$T = T_m \sin^2 \theta/2 \qquad (2.4\ b)$$

The minimum energy transfer, for a collision at grazing incident is zero. But for our later calculations we will consider a cut-off energy as the minimum energy transfer to overcome the singularities that appear in the integrals for the cross-sections as will be seen in Chapter 3.

The energy E_2 retained by the primary in a collision of deflection angle θ in thus

$$E_2 = E_o[1 - (1 - \alpha) \sin^2 \theta/2] \qquad (2.5\ a)$$

The deflection angle in the lab. system can be found from the vector resolution in figure 2.2, which leads to the relation

$$\cos \psi = 1/2 \left\{(1 + A) \left(\frac{E_2}{E_o}\right)^{1/2} + (1 - A) \left(\frac{E_o}{E_2}\right)^{1/2}\right\} \qquad (2.6\ a)$$

or in terms of the C.M. system scattering angle,

$$\cos \psi = \frac{A \cos \theta + 1}{[A^2 + 2A \cos \theta + 1]^{1/2}} \qquad (2.6\ b)$$

Now, how can we calculate the scattering angle in the C.M. system for a given interaction potential between the incoming particle and the struck atom. The interaction force between collision partners F(r) can be thought of as composed of two terms: one attractive, which is of importance only at large interatomic distances and represents the cohesive forces which bind the crystal, the other which is repulsive dominates over the close interaction distances with which we are concerned. The repulsive force increases rapidly with decreasing internuclear distance. If the interatomic potential is represented by V(r), therefore $F(r) = \frac{\partial}{\partial r}\{V(r)\}$ increases rapidly at low separations between the forces centres. G. Carter and J.S. Colligon present the expression for the scattering angle θ in C.M. System which is

$$\theta = \pi - 2p \int_0^{u_o} \frac{du}{\left[1 - \frac{V(u)}{E_R} - p^2u^2\right]} \qquad (2.7)$$

where p is the impact parameter, $u \equiv \frac{1}{r}$, and E_R is the primary energy measured with respect to the centre of mass, i.e.

$$E_R = E_o - \frac{M_1}{M_1 + M_2} E_o = \frac{A}{1 + A} E_o \qquad (2.8)$$

for a real primary energy E_o, and u_o is the value of u for which the denominator of equation (2.7) vanishes.

In this work we are considering the interaction potential V(r) is that of a Thomas-Fermi potential, which is given by Oen and Robinson (1964). We plug this potential in equation (2.7) and solve the transcendental equation,

$$1 - \frac{V(u_o)}{E_R} - p^2 u_o^2 = 0,$$

for u_o and then perform the integration numerically. But for computation convenience and saving computing time we use another approach to calculate the scattering angle in the C.M. system depending on the use of random numbers for determining the fraction of maximum energy transferred and from the relation between the scattering angle θ and the energy transferred, equation (2.4 b), we can determine the scattering angle. This will be shown in Chapter 3.

2.2.2 Thomas-Fermi Cross Section:

The differential cross section for energy transfer for a Thomas-Fermi interaction potential, Winterbon et al. (1970), is given by,

$$d\sigma = \pi a^2 \frac{dt}{2t^{3/2}} f(t^{1/2}) \qquad (2.9\ a)$$

where

$$t = \varepsilon^2 T/T_m,$$

$$T_m = \gamma E,$$

E = initial energy,

T = recoil energy, $0 \leq T \leq T_m$,

$$\gamma = 4 M_1 M_2/(M_1 + M_2)^2, \qquad (2.9\ b)$$

M_1 = mass of incident particle,

M_2 = mass of struck atom,

$$\varepsilon = \left(\frac{M_2 E}{M_1 + M_2}\right) \left(\frac{Z_1 Z_2 e^2}{a}\right)^{-1},$$

Z_1 = atomic number of incident particle,

Z_2 = atomic number of struck atom,

a = screening radius,

$f(t^{1/2})$ is a function that depends on the assumed form of the screening function

We shall follow Linhard et al. (1968) and use the screening radius

$$a = 0.8853\, a_o\, Z^{-1/3} \tag{2.10 a}$$

where

$$Z^{2/3} = Z_1^{2/3} + Z_2^{2/3}$$
$$a_o = \hbar^2/me^2 = 0.529\ \text{Å} \tag{2.10 b}$$

The function $f(t^{1/2})$ has been calculated for the collison of neutral Thomas-Fermi atoms. The following analytic approximation will be used,

$$f(t^{1/2}) = 1.309\, t^{1/6}\, [1 + (2.618\, t^{2/3})^{2/3}]^{-3/2} \tag{2.11}$$

we have from (2.9 b),

$$t = \varepsilon^2\, T/T_m = \varepsilon^2 x$$

where $x = T/T_m$, and hence we get

$$dt = \varepsilon^2 dx$$

Substituting back in equation (2.9 a), we have

$$d\sigma = \pi a^2 .\, \frac{\varepsilon^2 dx}{2\, \varepsilon^3\, x^{3/2}}\, f(x,\varepsilon)$$

where

$$f(x,\varepsilon) = 1.309 \frac{(\varepsilon^2 x)^{1/6}}{[1 + (2.618\ \varepsilon^{4/3}\ x^{2/3})^{2/3}]^{3/2}}$$

Therefore,

$$d\sigma = \frac{1.309}{2}\ \pi a^2 \frac{dx}{\varepsilon^{2/3}\ x^{4/3}[1 + (2.618\ \varepsilon^{4/3}\ x^{2/3})^{2/3}]^{3/2}} \qquad (2.12)$$

Now, to get the total cross section, we integrate over all possible values of x, i.e., all possible values of energy transferred.

Since T varies from 0 to T_m, therefore x must vary from 0 to 1. Hence,

$$\sigma = 0.6545\ \pi a^2 \int_0^1 \frac{dx}{\varepsilon^{2/3}\ x^{4/3}[1 + (2.618\ \varepsilon^{4/3}\ x^{2/3})^{2/3}]^{3/2}} \qquad (2.13)$$

As we see the integral in the R.H.S. does not depend on the specific collision partners, and we will perform it first for different values of the reduced energy ε, and call this integral $Y(\varepsilon)$

$$Y(\varepsilon) = \int_0^1 \frac{dx}{\varepsilon^{2/3}\ x^{4/3}[1 + (2.618\ \varepsilon^{4/3}\ x^{2/3})^{2/3}]^{3/2}} \qquad (2.14)$$

We notice that at the lower limit of the integral we will have a singularity. To overcome this singularity we determine a cut-off energy by assuming that the potential tends to zero at R_c which is the atomic radius, instead of infinity, a reasonable value of x that gives resonable results is taken as $x_{min} = 0.001$, i.e.

$$Y(\varepsilon) = \int_{0.001}^{1} \frac{dx}{\varepsilon^{2/3}\, x^{4/3}\left[1 + (2.618\, \varepsilon^{4/3}\, x^{2/3})^{2/3}\right]^{3/2}} \qquad (2.15)$$

Now, since the energy E and the reduced energy ε are related as shown in (2.9 b), therefore we can find the values of E which correspond to the calculated values of $Y(\varepsilon)$, in other words, we can obtain $Y'(E)$. But these values of $Y'(E)$ will differ from $Y(\varepsilon)$ in the sense that it depends on the collision partners.

2.3 Electronic Energy Loss:

At low energies ionic collisions with atoms are largely elastic. But at higher ion energies the electronic excitation becomes increasingly important. The rate of loss of energy to electrons has been calculated by Linhard and Sharff (1961) using a statistical model, and a simple analytical form has been obtained for the range of velocities $v \lesssim v_0$ (where v_0 is the velocity of an electron in the first Bohr orbit). In the case of hydrogen ions moving in solids, the electron loss process is dominant above energies of 1 Kev (while $v = v_0$ at 25 Kev). However, this does not preclude the possibility of a small number of scattering collisions, and where such collisions give rise to large angular deflections then reflection or back-scattering of incident ions can occur.

The rate of electronic energy loss that will be used in the forthcoming calculations is that given by McCracken and Freeman (1969) based on the theory of Linhard and Scharff.

$$\frac{dE}{dx} = - K\, E^{1/2} \qquad (2.16)$$

where K is a constant given by,

$$K = Z_1^{1/6} \frac{Z_1 Z_2}{(Z_1^{2/3} + Z_2^{2/3})^{3/2}} 8 \pi N e^2 a_o \left(\frac{1}{E'}\right)^{1/2} \qquad (2.17)$$

where N is the density of ions in the solid, a_o the Bohr radius and E' is the energy at which the ion velocity equals the velocity of an electron in the first Bohr orbit, this equals 25 Kev for hydrogen.

From equation (2.16) we obtain the energy of the ion for any distance x travelled within the solid,

$$E(x) = (\sqrt{E_o} - \frac{1}{2} K x)^2 \qquad (2.18)$$

where E_o is the initial ion energy.

We see from equations (2.16) and (2.18) that the electronic energy loss is a continuous process throughout the path of the particle, whereas the nuclear collisions are not continuous and happen according to certain interaction cross sections, so in the next chapter we will establish a model for the two energy loss processes.

CHAPTER 3

Projected Range and Back-scattering

3.1 Introduction

This is the major chapter in which we will develop a model for calculating the back-scattering of hydrogen ions. Here we consider both energy loss mechanisms, namely, electronic energy loss and nuclear collisions energy loss. The main idea is to develop a scheme that takes into account the continuous energy decrease of ions due to electron interactions, and consequently the continuously changing nuclear collision cross section. We make use of the random number technique as will be shown. The nuclear collision cross section is that for a Thomas-Fermi potential.

3.2 Calculation of Nuclear Collision Positions:

The usual way to find the nuclear collision location is the use of the mean free path concept. The mean free path, which is the average distance between interactions, is the reciprocal of the macroscopic scattering cross section which is energy dependent, and so will be continuously varying in our case due to electronic energy loss. The alternative scheme which will be used in our calculations is developed as follows:

From the continuous energy loss due to electronic collisions, we have

$$E(x) = (\sqrt{E_o} - \frac{1}{2} K x) \qquad (3.1)$$

K is the constant defined in Chapter 2.

The ion will move in the solid until its energy reaches a minimum value, this value will be taken 25 ev which corresponds to the threshold energy for atomic displacement, at this energy we consider the ion to be absorbed. If we assume that the distance at which the ion is absorbed is x_{max} which corresponds to ion energy E_{min} = 25 ev. The probability of at least one nuclear scattering occurs is P_N and is given by,

$$P_N = 1 - \exp \{ - \int_0^{x_{max}} N \sigma(E) \, dx' \} \qquad (3.2)$$

where N is the atomic density of the target material, and $\sigma(E)$ is the scattering cross section as a function of energy (and consequently a function of distance). This probability varies from 0 to 1, and so if we choose a random number q, therefore, if $q \geq P_N$, no nuclear scattering will occur and if $q < P_N$, we will have at least one nuclear scattering. Hence, the probability that we have a nuclear scattering at distance x ($< x_{max}$) is given by,

$$q = 1 - \exp \{ - \int_0^{x} N \sigma(E) \, dx' \} \qquad (3.3)$$

Since,

$$\int_0^{x_{max}} N \sigma(E) \, dx' = \int_0^{x} N \sigma(E) \, dx' + \int_x^{x_{max}} N \sigma(E) \, dx'$$

therefore equation (3.3) becomes,

$$q = 1 - \exp \{ - \int_0^{x_{max}} N \sigma(E) \, dx' + \int_x^{x_{max}} N \sigma(E) \, dx' \}$$

$$q = 1 - \exp\left\{ - \int_{o}^{x_{max}} N\,\sigma(E)\,dx' \right\} \exp\left\{ \int_{x}^{x_{max}} N\,\sigma(E)\,dx' \right\} \qquad (3.4)$$

Therefore, substituting from equation (3.2) into equation (3.4), we have

$$q = 1 - (1 - P_N) \exp\left\{ \int_{x}^{x_{max}} N\,\sigma(E)\,dx' \right\} \qquad (3.5)$$

From which we get,

$$\int_{x}^{x_{max}} N\,\sigma(E)\,dx' = \ln\left[\frac{1 - q}{1 - P_N}\right] \qquad (3.6)$$

But we have for the continuous energy loss due to electronic collisions,

$$\frac{dE}{dx} = - K\,E^{1/2}$$

Therefore, changing variables in equation (3.6) we obtain

$$\int_{E(x)}^{E(x_{max})} - \frac{N\,\sigma(E')\,dE'}{K(E')^{1/2}} = \ln\left[\frac{1 - q}{1 - P_N}\right]$$

i.e.

$$\int_{E_{min}}^{E(x)} \frac{N\,\sigma(E')\,dE'}{K(E')^{1/2}} = \ln\left[\frac{1 - q}{1 - P_N}\right] \qquad (3.7)$$

If we put the integral in L.H.S. of equation (3.7) by the expression R(E) Therefore,

$$R(E) = \int_{E_{min}}^{E} \frac{N\,\sigma(E')\,dE'}{K(E')^{1/2}} \tag{3.8}$$

Now, we can rewrite equations (3.2) as

$$P_N = 1 - \exp\{ - \int_{E_{min}}^{E_o} \frac{N\,\sigma(E')\,dE'}{K(E')^{1/2}} \} = 1 - \exp\{ - R(E_o)\} \tag{3.9}$$

and going back to equation (3.5) we get

$$q = 1 - (1 - P_N) \exp\{R(E)\}$$

$$= 1 - \exp\{- R(E_o)\} \exp\{R(E)\}$$

$$= 1 - \exp\{R(E) - R(E_o)\}$$

Therefore

$$R(E) - R(E_o) = \ln [1 - q] \tag{3.10}$$

To summarize the equations that will be used in the calculation we find that we will deal with the following four equations,

$$E(x) = (\sqrt{E_o} - \frac{1}{2} K x)^2 \tag{3.1}$$

$$R(E) = \int_{E_{min}}^{E} \frac{N\,\sigma(E')\,dE'}{K(E')^{1/2}} \tag{3.8}$$

$$P_N = 1 - \exp\{-R(E_o)\} \tag{3.9}$$

and

$$R(E) - R(E_o) = \ln[1 - q] \tag{3.10}$$

Now, we can set up the steps to be followed for determining the nuclear scattering positions:

1. We tabulate values of R(E) for different energies from equation (3.8)
2. We determine P_N from $R(E_o)$, equation (3.9)
3. Choose a random number q and check $q < P_N$
4. From equation (3.10) we find R(E), and consequently E(x) from the first step.
5. Using equation (3.1) we can determine the position of nuclear scattering x after knowing E(x) from the fourth step.

3.2.1 Tabulation of R(E):

For the tabulation of R(E) for different values of energies we have to evaluate the integral,

$$R(E) = \int_{E_{min}}^{E} \frac{N\,\sigma(E')\,dE'}{K(E')^{1/2}}$$

This can be done in two steps, the first is to evaluate the cross section $\sigma(E')$

for different values of energies, this was done in (2.2.3), and then plug these values of $\sigma(E')$ in the above integral to evaluate R(E).

Hence, the integral for R(E) takes the form,

$$R(E) = \frac{0.6545\ \pi a^2\ N}{K} \int_{E_{min}}^{E} \frac{Y(E')}{(E')^{1/2}}\ dE'$$

if we put $F(E') = Y(E')/(E')^{1/2}$, therefore

$$R(E) = \frac{0.6545\ \pi a^2\ N}{K} \int_{E_{min}}^{E} F(E')\ dE' \qquad (3.11)$$

Now, we can calculate the values of R(E) for different values of energies. So, we can go through all the steps required to determine the nuclear collision location.

3.3 Scattering Angle in the C.M. System:

To calculate the scattering angle in C.M. system θ, we have to evaluate the integral in equation (2.7)

$$\theta = \pi - 2p \int_{o}^{u_o} \frac{du}{\left[1 - \frac{v(u)}{E_R} - p^2u^2\right]}$$

and as we saw, this requiresthe solution of a transcendental equation to evaluate the value of the upper limit of the integral u_o. Since, for the Thomas-Fermi

potential we will not be able to evaluate the integral analytically, therefore we will suggest another alternative scheme for the calculation of θ.

We have the differential scattering cross section for energy transfer in equation (2.12). Since the energy transferred T varies from T_{min} (the cut-off energy) to T_m (the maximum energy transferred) and consequently x varies from x_{min} to 1. Therefore we find that the ratio

$$\frac{\int_{T_{min}}^{T} d\sigma}{\int_{T_{min}}^{T_m} d\sigma}$$

will vary from zero to 1. Choosing a random number q' which is uniformly distributed from zero to 1, we find

$$q' = \frac{\int_{T_{min}}^{T} d\sigma}{\int_{T_{min}}^{T_m} d\sigma} \tag{3.12}$$

The denominator of this equation is actually the total scattering cross section. Equation (3.12) can be rewritten in the form,

$$q' Y(\varepsilon) = \int_{0.001}^{X} \frac{dx}{\varepsilon^{2/3}\, x^{3/2}\, [1 + (2.1618\, \varepsilon^{4/3}\, x^{2/3})^{2/3}]^{3/2}} \tag{3.13}$$

The integral on the R.H.S. of equation (3.13) is evaluated for different values of x. So, according to any random number q' we can find the value of x which satisfied equation (3.13). We assumed that,

$$x = T/T_m$$

and therefore by using equation (2.4 b), we find that

$$\sin^2 (\theta/2) = x \qquad (3.14)$$

from this equation we can find the scattering angle in the C.M. system θ.

3.3.1 Nuclear Scattering Collisions in the Lab. System:

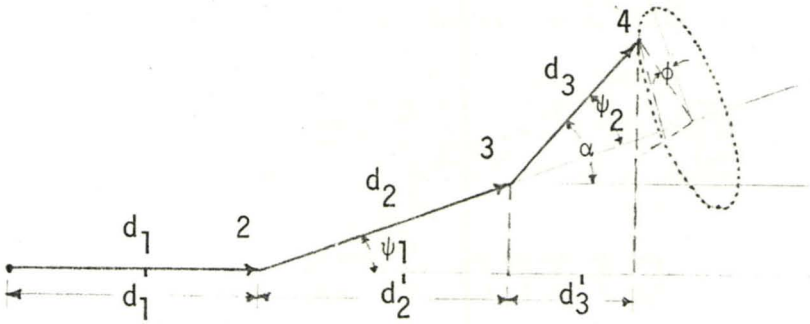

Fig. 3.1: Ion transport inside the solid

In figure 3.1 we represent two collision processes. The particle begins at point 1 (at the surface) with energy E_o. By calculating the location of first collision as explained before, we can determine the energy of the particle before and after collision at point 2. The angular deflection ψ, from the original direction is determined from equation (2.6 b). Then we repeat the same steps to determine the second scattering event at point 3. At this point we have, in addition to the deflection angle ψ_2, an azimuthal angle ϕ which varies from 0 to 2π. Therefore by choosing a random number q'' we find that the angle ϕ is determined by,

$$\phi = q'' . 2\pi \qquad (3.15)$$

To find the projected range of the particle we evaluate the projection of each traversed distance on the original direction. So the projected range before the second collision is given by, d, where

$$d = d_1 + d_2 \cos \psi_1 \tag{3.16}$$

and before the third collision d is given by,

$$d = d_1 + d_2 \cos \psi_1 + d_3 \cos \alpha \tag{3.17 a}$$

where the angle α is found from the equation,

$$\cos \alpha = \cos \psi_1 \cos \psi_2 + \sin \psi_1 \sin \psi_2 \cos \phi \tag{3.17 b}$$

For computational work we put $\psi_1 = \alpha$, before the third collision and proceed in the same previous way.

3.4 Description of the Complete Computation Work:

This section may be a summary of the whole work described before, and in addition to this we describe the calculated parameters and method of calculations.

First for the given initial energy E_o we determine the first nuclear collision location, and evaluate the energies before and after the collision. In the same way we proceed to the second and third collision, ... etc. At each point we calculate the projected range from equation (3.17 a). Also, at each location we check whether the projected range is negative or positive, in the former case, the particle is back-scattered and in this case, we determine the back-scattered energy and back-scattering angle that the outgoing particle

makes with the original direction. To find the back-scattered energy we first determine the distance from the last scattering to the surface, DS, if we assume that we are considering the scattering number J, therefore

$$DS = d(J-1)/\cos \psi_1 \qquad (3.18)$$

and the back-scattered energy will be given by equation (3.1), where x = DS. If, on the other hand, the projected range is positive we check the particle energy with a certain minimum value, taken in our work as 1 Kev, this is done just for saving computer time. In the exact case, we must consider all interactions until particle energy reaches minimum value, namely, 25 ev.

After finishing the history of the first particle we repeat the same procedure with the remaining particles, with the same initial conditions, and therefore will be able to find the average number of back-scattered particles and their energy and angular distribution.

Also, the same work will be repeated for different initial energies to discuss the effect of initial particle energy on the ions back-scattering.

Chapter 4

Sample Calculation

4.1 Results:

In this chapter the computation results are listed and plots for the outputs are also given. In these calculations, we are considering two different cases for the initial energy of the incident particles, namely, 5 Kev and 10 Kev hydrogen ions and the target material is aluminum.

For the calculation of reflected particles we consider collisions until the projected range reaches 500 Angstroms for the 5 Kev particles and 1000 Angstroms for the 10 Kev case. Also, we are considering the whole range of particles for the calculation of the projected range for the 10 Kev ions to be compared with the work of Schiott (1966) as a check for our work. In both cases, we are considering interactions only for energies greater than 1 Kev. These approximations are made only to save computer time, since each run takes a considerable amount of computer time.

The computer programmes that were used in this work for calculating Y, R, reflection, and projected range will be listed in the appendix.

ε	E	Y
.100000E-01	.105809E-01	.576859E+03
.200000E-01	.211619E-01	.360853E+03
.300000E-01	.317428E-01	.273591E+03
.400000E-01	.423237E-01	.224450E+03
.500000E-01	.529046E-01	.192279E+03
.600000E-01	.634856E-01	.169299E+03
.700000E-01	.740665E-01	.151918E+03
.800000E-01	.846474E-01	.138230E+03
.900000E-01	.952283E-01	.127119E+03
.100000E+00	.105809E+00	.117888E+03
.110000E+00	.116390E+00	.110075E+03
.120000E+00	.126971E+00	.103360E+03
.130000E+00	.137552E+00	.975162E+02
.140000E+00	.148133E+00	.923755E+02
.150000E+00	.158714E+00	.878120E+02
.160000E+00	.169295E+00	.837286E+02
.170000E+00	.179876E+00	.800495E+02
.180000E+00	.190457E+00	.767145E+02
.190000E+00	.201038E+00	.736748E+02
.200000E+00	.211619E+00	.708910E+02
.210000E+00	.222199E+00	.683303E+02
.220000E+00	.232780E+00	.659656E+02
.230000E+00	.243361E+00	.637740E+02
.240000E+00	.253942E+00	.617363E+02
.250000E+00	.264523E+00	.598359E+02
.260000E+00	.275104E+00	.580588E+02
.270000E+00	.285685E+00	.563926E+02
.280000E+00	.296266E+00	.548268E+02
.290000E+00	.306847E+00	.533522E+02
.300000E+00	.317428E+00	.519606E+02

ϵ	E	Y
.310000E+00	.328009E+00	.506448E+02
.320000E+00	.338590E+00	.493985E+02
.330000E+00	.349171E+00	.482161E+02
.340000E+00	.359752E+00	.470925E+02
.350000E+00	.370332E+00	.460232E+02
.360000E+00	.380913E+00	.450043E+02
.370000E+00	.391494E+00	.440320E+02
.380000E+00	.402075E+00	.431031E+02
.390000E+00	.412656E+00	.422147E+02
.400000E+00	.423237E+00	.413639E+02
.410000E+00	.433818E+00	.405484E+02
.420000E+00	.444399E+00	.397658E+02
.430000E+00	.454980E+00	.390142E+02
.440000E+00	.465561E+00	.382917E+02
.450000E+00	.476142E+00	.375965E+02
.460000E+00	.486723E+00	.369271E+02
.470000E+00	.497304E+00	.362819E+02
.480000E+00	.507885E+00	.356597E+02
.490000E+00	.518465E+00	.350591E+02
.500000E+00	.529046E+00	.344790E+02
.510000E+00	.539627E+00	.339184E+02
.520000E+00	.550208E+00	.333762E+02
.530000E+00	.560789E+00	.328515E+02
.540000E+00	.571370E+00	.323434E+02
.550000E+00	.581951E+00	.318512E+02
.560000E+00	.592532E+00	.313740E+02
.570000E+00	.603113E+00	.309112E+02
.580000E+00	.613694E+00	.304620E+02
.590000E+00	.624275E+00	.300260E+02
.600000E+00	.634856E+00	.296024E+02

ε	E	Y
.610000E+00	.645437E+00	.291907E+02
.620000E+00	.656018E+00	.287905E+02
.630000E+00	.666598E+00	.284012E+02
.640000E+00	.677179E+00	.280224E+02
.650000E+00	.687760E+00	.276536E+02
.660000E+00	.698341E+00	.272944E+02
.670000E+00	.708922E+00	.269445E+02
.680000E+00	.719503E+00	.266035E+02
.690000E+00	.730084E+00	.262710E+02
.700000E+00	.740665E+00	.259468E+02
.710000E+00	.751246E+00	.256304E+02
.720000E+00	.761827E+00	.253216E+02
.730000E+00	.772408E+00	.250201E+02
.740000E+00	.782989E+00	.247258E+02
.750000E+00	.793570E+00	.244382E+02
.760000E+00	.804150E+00	.241571E+02
.770000E+00	.814731E+00	.238824E+02
.780000E+00	.825312E+00	.236138E+02
.790000E+00	.835893E+00	.233512E+02
.800000E+00	.846474E+00	.230942E+02
.810000E+00	.857055E+00	.228428E+02
.820000E+00	.867636E+00	.225966E+02
.830000E+00	.878217E+00	.223557E+02
.840000E+00	.888798E+00	.221197E+02
.850000E+00	.899379E+00	.218886E+02
.860000E+00	.909960E+00	.216622E+02
.870000E+00	.920541E+00	.214403E+02
.880000E+00	.931122E+00	.212228E+02
.890000E+00	.941703E+00	.210096E+02
.900000E+00	.952283E+00	.208005E+02

ϵ	E	Y
.910000E+00	.962864E+00	.205955E+02
.920000E+00	.973445E+00	.203943E+02
.930000E+00	.984026E+00	.201970E+02
.940000E+00	.994607E+00	.200033E+02
.950000E+00	.100519E+01	.198132E+02
.960000E+00	.101577E+01	.196265E+02
.970000E+00	.102635E+01	.194433E+02
.980000E+00	.103693E+01	.192633E+02
.990000E+00	.104751E+01	.190865E+02
.100000E+01	.105809E+01	.189128E+02
.110000E+01	.116390E+01	.173301E+02
.120000E+01	.126971E+01	.159826E+02
.130000E+01	.137552E+01	.148209E+02
.140000E+01	.148133E+01	.138084E+02
.150000E+01	.158714E+01	.129179E+02
.160000E+01	.169295E+01	.121283E+02
.170000E+01	.179876E+01	.114233E+02
.180000E+01	.190457E+01	.107899E+02
.190000E+01	.201038E+01	.102176E+02
.200000E+01	.211619E+01	.969813E+01
.210000E+01	.222199E+01	.922438E+01
.220000E+01	.232780E+01	.879061E+01
.230000E+01	.243361E+01	.839197E+01
.240000E+01	.253942E+01	.802440E+01
.250000E+01	.264523E+01	.768441E+01
.260000E+01	.275104E+01	.736905E+01
.270000E+01	.285685E+01	.707575E+01
.280000E+01	.296266E+01	.680232E+01
.290000E+01	.306847E+01	.654682E+01
.300000E+01	.317428E+01	.630757E+01

ϵ	E	Y
.310000E+01	.328009E+01	.608309E+01
.320000E+01	.338590E+01	.587209E+01
.330000E+01	.349171E+01	.567340E+01
.340000E+01	.359752E+01	.548600E+01
.350000E+01	.370332E+01	.530897E+01
.360000E+01	.380913E+01	.514151E+01
.370000E+01	.391494E+01	.498286E+01
.380000E+01	.402075E+01	.483237E+01
.390000E+01	.412656E+01	.468945E+01
.400000E+01	.423237E+01	.455355E+01
.410000E+01	.433818E+01	.442418E+01
.420000E+01	.444399E+01	.430090E+01
.430000E+01	.454980E+01	.418330E+01
.440000E+01	.465561E+01	.407100E+01
.450000E+01	.476142E+01	.396368E+01
.460000E+01	.486723E+01	.386101E+01
.470000E+01	.497304E+01	.376272E+01
.480000E+01	.507885E+01	.366853E+01
.490000E+01	.518465E+01	.357821E+01
.500000E+01	.529046E+01	.349153E+01
.510000E+01	.539627E+01	.340828E+01
.520000E+01	.550208E+01	.332828E+01
.530000E+01	.560789E+01	.325134E+01
.540000E+01	.571370E+01	.317729E+01
.550000E+01	.581951E+01	.310599E+01
.560000E+01	.592532E+01	.303730E+01
.570000E+01	.603113E+01	.297107E+01
.580000E+01	.613694E+01	.290718E+01
.590000E+01	.624275E+01	.284552E+01
.600000E+01	.634856E+01	.278598E+01

ϵ	E	Y
.610000E+01	.645437E+01	.272845E+01
.620000E+01	.656018E+01	.267284E+01
.630000E+01	.666598E+01	.261906E+01
.640000E+01	.677179E+01	.256703E+01
.650000E+01	.687760E+01	.251666E+01
.660000E+01	.698341E+01	.246789E+01
.670000E+01	.708922E+01	.242063E+01
.680000E+01	.719503E+01	.237483E+01
.690000E+01	.730084E+01	.233042E+01
.700000E+01	.740665E+01	.228734E+01
.710000E+01	.751246E+01	.224554E+01
.720000E+01	.761827E+01	.220497E+01
.730000E+01	.772408E+01	.216556E+01
.740000E+01	.782989E+01	.212729E+01
.750000E+01	.793570E+01	.209009E+01
.760000E+01	.804150E+01	.205394E+01
.770000E+01	.814731E+01	.201878E+01
.780000E+01	.825312E+01	.198458E+01
.790000E+01	.835893E+01	.195131E+01
.800000E+01	.846474E+01	.191892E+01
.810000E+01	.857055E+01	.188739E+01
.820000E+01	.867636E+01	.185668E+01
.830000E+01	.878217E+01	.182677E+01
.840000E+01	.888798E+01	.179763E+01
.850000E+01	.899379E+01	.176922E+01
.860000E+01	.909960E+01	.174152E+01
.870000E+01	.920541E+01	.171452E+01
.880000E+01	.931122E+01	.168817E+01
.890000E+01	.941703E+01	.166247E+01
.900000E+01	.952283E+01	.163739E+01

G	E	Y
.910000E+01	.962864E+01	.161291E+01
.920000E+01	.973445E+01	.158900E+01
.930000E+01	.984026E+01	.156566E+01
.940000E+01	.994607E+01	.154285E+01
.950000E+01	.100519E+02	.152058E+01
.960000E+01	.101577E+02	.149881E+01
.970000E+01	.102635E+02	.147753E+01
.980000E+01	.103693E+02	.145673E+01
.990000E+01	.104751E+02	.143639E+01
.100000E+02	.105809E+02	.141649E+01
.101000E+02	.106867E+02	.139703E+01
.102000E+02	.107925E+02	.137800E+01
.103000E+02	.108984E+02	.135937E+01
.104000E+02	.110042E+02	.134113E+01
.105000E+02	.111100E+02	.132328E+01
.106000E+02	.112158E+02	.130581E+01
.107000E+02	.113216E+02	.128869E+01
.108000E+02	.114274E+02	.127193E+01
.109000E+02	.115332E+02	.125551E+01
.110000E+02	.116390E+02	.123942E+01
.111000E+02	.117448E+02	.122366E+01
.112000E+02	.118506E+02	.120821E+01
.113000E+02	.119564E+02	.119307E+01
.114000E+02	.120623E+02	.117822E+01
.115000E+02	.121681E+02	.116367E+01
.116000E+02	.122739E+02	.114939E+01
.117000E+02	.123797E+02	.113539E+01
.118000E+02	.124855E+02	.112165E+01
.119000E+02	.125913E+02	.110818E+01
.120000E+02	.126971E+02	.109496E+01

ε	E	Y
.121000E+02	.128029E+02	.108198E+01
.122000E+02	.129087E+02	.106925E+01
.123000E+02	.130145E+02	.105675E+01
.124000E+02	.131204E+02	.104447E+01
.125000E+02	.132262E+02	.103242E+01
.126000E+02	.133320E+02	.102059E+01
.127000E+02	.134378E+02	.100897E+01
.128000E+02	.135436E+02	.997551E+00
.129000E+02	.136494E+02	.986337E+00
.130000E+02	.137552E+02	.975319E+00
.131000E+02	.138610E+02	.964492E+00
.132000E+02	.139668E+02	.953853E+00
.133000E+02	.140726E+02	.943397E+00
.134000E+02	.141784E+02	.933119E+00
.135000E+02	.142843E+02	.923015E+00
.136000E+02	.143901E+02	.913082E+00
.137000E+02	.144959E+02	.903314E+00
.138000E+02	.146017E+02	.893710E+00
.139000E+02	.147075E+02	.884263E+00
.140000E+02	.148133E+02	.874972E+00
.141000E+02	.149191E+02	.865833E+00
.142000E+02	.150249E+02	.856842E+00
.143000E+02	.151307E+02	.847996E+00
.144000E+02	.152365E+02	.839292E+00
.145000E+02	.153423E+02	.830726E+00
.146000E+02	.154482E+02	.822296E+00
.147000E+02	.155540E+02	.813999E+00
.148000E+02	.156598E+02	.805831E+00
.149000E+02	.157656E+02	.797791E+00
.150000E+02	.158714E+02	.789875E+00

ε	E	Y
.151000E+02	.159772E+02	.782080E+00
.152000E+02	.160830E+02	.774405E+00
.153000E+02	.161888E+02	.766847E+00
.154000E+02	.162946E+02	.759402E+00
.155000E+02	.164004E+02	.752070E+00
.156000E+02	.165062E+02	.744847E+00
.157000E+02	.166121E+02	.737732E+00
.158000E+02	.167179E+02	.730722E+00
.159000E+02	.168237E+02	.723815E+00
.160000E+02	.169295E+02	.717008E+00
.161000E+02	.170353E+02	.710301E+00
.162000E+02	.171411E+02	.703691E+00
.163000E+02	.172469E+02	.697176E+00
.164000E+02	.173527E+02	.690754E+00
.165000E+02	.174585E+02	.684424E+00
.166000E+02	.175643E+02	.678183E+00
.167000E+02	.176701E+02	.672030E+00
.168000E+02	.177760E+02	.665963E+00
.169000E+02	.178818E+02	.659981E+00
.170000E+02	.179876E+02	.654082E+00
.171000E+02	.180934E+02	.648264E+00
.172000E+02	.181992E+02	.642526E+00
.173000E+02	.183050E+02	.636867E+00
.174000E+02	.184108E+02	.631284E+00
.175000E+02	.185166E+02	.625777E+00
.176000E+02	.186224E+02	.620344E+00
.177000E+02	.187282E+02	.614984E+00
.178000E+02	.188341E+02	.609695E+00
.179000E+02	.189399E+02	.604476E+00
.180000E+02	.190457E+02	.599326E+00

ϵ	E	Y
.181000E+02	.191515E+02	.594243E+00
.182000E+02	.192573E+02	.589228E+00
.183000E+02	.193631E+02	.584277E+00
.184000E+02	.194689E+02	.579390E+00
.185000E+02	.195747E+02	.574566E+00
.186000E+02	.196805E+02	.569804E+00
.187000E+02	.197863E+02	.565103E+00
.188000E+02	.198921E+02	.560462E+00
.189000E+02	.199980E+02	.555879E+00
.190000E+02	.201038E+02	.551354E+00
.191000E+02	.202096E+02	.546886E+00
.192000E+02	.203154E+02	.542473E+00
.193000E+02	.204212E+02	.538115E+00
.194000E+02	.205270E+02	.533811E+00
.195000E+02	.206328E+02	.529560E+00
.196000E+02	.207386E+02	.525361E+00
.197000E+02	.208444E+02	.521213E+00
.198000E+02	.209502E+02	.517115E+00
.199000E+02	.210560E+02	.513067E+00
.200000E+02	.211619E+02	.509068E+00
.201000E+02	.212677E+02	.505116E+00
.202000E+02	.213735E+02	.501212E+00
.203000E+02	.214793E+02	.497354E+00
.204000E+02	.215851E+02	.493541E+00
.205000E+02	.216909E+02	.489774E+00
.206000E+02	.217967E+02	.486051E+00
.207000E+02	.219025E+02	.482371E+00
.208000E+02	.220083E+02	.478734E+00
.209000E+02	.221141E+02	.475138E+00
.210000E+02	.222199E+02	.471585E+00

ϵ	E	Y
.211000E+02	.223258E+02	.468072E+00
.212000E+02	.224316E+02	.464599E+00
.213000E+02	.225374E+02	.461166E+00
.214000E+02	.226432E+02	.457772E+00
.215000E+02	.227490E+02	.454416E+00
.216000E+02	.228548E+02	.451098E+00
.217000E+02	.229606E+02	.447817E+00
.218000E+02	.230664E+02	.444573E+00
.219000E+02	.231722E+02	.441364E+00
.220000E+02	.232780E+02	.438191E+00
.221000E+02	.233838E+02	.435053E+00
.222000E+02	.234897E+02	.431950E+00
.223000E+02	.235955E+02	.428880E+00
.224000E+02	.237013E+02	.425844E+00
.225000E+02	.238071E+02	.422841E+00
.226000E+02	.239129E+02	.419870E+00
.227000E+02	.240187E+02	.416931E+00
.228000E+02	.241245E+02	.414024E+00
.229000E+02	.242303E+02	.411148E+00
.230000E+02	.243361E+02	.408302E+00
.231000E+02	.244419E+02	.405487E+00
.232000E+02	.245478E+02	.402701E+00
.233000E+02	.246536E+02	.399944E+00
.234000E+02	.247594E+02	.397217E+00
.235000E+02	.248652E+02	.394518E+00
.236000E+02	.249710E+02	.391847E+00
.237000E+02	.250768E+02	.389203E+00
.238000E+02	.251826E+02	.386587E+00
.239000E+02	.252884E+02	.383998E+00
.240000E+02	.253942E+02	.381435E+00

ϵ	E	Y
.241000E+02	.255000E+02	.378899E+00
.242000E+02	.256058E+02	.376388E+00
.243000E+02	.257117E+02	.373903E+00
.244000E+02	.258175E+02	.371443E+00
.245000E+02	.259233E+02	.369008E+00
.246000E+02	.260291E+02	.366597E+00
.247000E+02	.261349E+02	.364210E+00
.248000E+02	.262407E+02	.361847E+00
.249000E+02	.263465E+02	.359507E+00
.250000E+02	.264523E+02	.357190E+00
.251000E+02	.265581E+02	.354897E+00
.252000E+02	.266639E+02	.352625E+00
.253000E+02	.267697E+02	.350376E+00
.254000E+02	.268756E+02	.348149E+00
.255000E+02	.269814E+02	.345944E+00
.256000E+02	.270872E+02	.343760E+00
.257000E+02	.271930E+02	.341596E+00
.258000E+02	.272988E+02	.339454E+00
.259000E+02	.274046E+02	.337332E+00
.260000E+02	.275104E+02	.335231E+00
.261000E+02	.276162E+02	.333149E+00
.262000E+02	.277220E+02	.331088E+00
.263000E+02	.278278E+02	.329045E+00
.264000E+02	.279336E+02	.327022E+00
.265000E+02	.280395E+02	.325018E+00
.266000E+02	.281453E+02	.323033E+00
.267000E+02	.282511E+02	.321066E+00
.268000E+02	.283569E+02	.319117E+00
.269000E+02	.284627E+02	.317187E+00
.270000E+02	.285685E+02	.315274E+00

ϵ	E	Y
.271000E+02	.286743E+02	.313379E+00
.272000E+02	.287801E+02	.311502E+00
.273000E+02	.288859E+02	.309641E+00
.274000E+02	.289917E+02	.307798E+00
.275000E+02	.290976E+02	.305971E+00
.276000E+02	.292034E+02	.304160E+00
.277000E+02	.293092E+02	.302366E+00
.278000E+02	.294150E+02	.300589E+00
.279000E+02	.295208E+02	.298827E+00
.280000E+02	.296266E+02	.297081E+00
.281000E+02	.297324E+02	.295350E+00
.282000E+02	.298382E+02	.293635E+00
.283000E+02	.299440E+02	.291935E+00
.284000E+02	.300498E+02	.290250E+00
.285000E+02	.301556E+02	.288580E+00
.286000E+02	.302615E+02	.286924E+00
.287000E+02	.303673E+02	.285283E+00
.288000E+02	.304731E+02	.283657E+00
.289000E+02	.305789E+02	.282044E+00
.290000E+02	.306847E+02	.280445E+00
.291000E+02	.307905E+02	.278861E+00
.292000E+02	.308963E+02	.277289E+00
.293000E+02	.310021E+02	.275732E+00
.294000E+02	.311079E+02	.274187E+00
.295000E+02	.312137E+02	.272656E+00
.296000E+02	.313195E+02	.271138E+00
.297000E+02	.314254E+02	.269633E+00
.298000E+02	.315312E+02	.268140E+00
.299000E+02	.316370E+02	.266660E+00
.300000E+02	.317428E+02	.265193E+00

ϵ	E	Y
.301000E+02	.318486E+02	.263738E+00
.302000E+02	.319544E+02	.262295E+00
.303000E+02	.320602E+02	.260864E+00
.304000E+02	.321660E+02	.259444E+00
.305000E+02	.322718E+02	.258037E+00
.306000E+02	.323776E+02	.256641E+00
.307000E+02	.324834E+02	.255257E+00
.308000E+02	.325893E+02	.253884E+00
.309000E+02	.326951E+02	.252522E+00
.310000E+02	.328009E+02	.251172E+00

E	R
.105809E+01	.323125E+03
.211619E+01	.350030E+03
.317428E+01	.361922E+03
.423237E+01	.368784E+03
.529046E+01	.373279E+03
.634856E+01	.376456E+03
.740665E+01	.378821E+03
.846474E+01	.380647E+03
.952283E+01	.382098E+03
.105809E+02	.383277E+03
.116390E+02	.384253E+03
.126971E+02	.385073E+03
.137552E+02	.385770E+03
.148133E+02	.386370E+03
.158714E+02	.386890E+03
.169295E+02	.387346E+03
.179876E+02	.387748E+03
.190457E+02	.388105E+03
.201038E+02	.388424E+03
.211619E+02	.388710E+03
.222199E+02	.388968E+03
.232780E+02	.389202E+03
.243361E+02	.389415E+03
.253942E+02	.389609E+03
.264523E+02	.389787E+03
.275104E+02	.389950E+03
.285685E+02	.390101E+03
.296266E+02	.390240E+03
.306847E+02	.390369E+03
.317428E+02	.390489E+03

Initial Energy: 5 Kev

Number of Particles: 1000

Particle Number	Back-scattered Energy, Kev	Back-scattering Angle, Degrees
4	1.69	33.8
20	0.56	66.9
83	1.14	53.6
110	1.65	38.9
146	0.17	51.5
191	1.42	48.9
284	1.15	21.8
314	1.94	47.9
323	0.06	81.1
333	1.71	50.8
389	1.29	45.0
442	1.34	32.4
464	1.17	79.3
476	2.20	58.9
559	1.28	11.4
567	1.61	44.8
575	1.43	44.7
607	2.44	37.4
680	2.81	51.2
705	1.99	46.6
766	1.84	39.0
863	1.26	6.6
996	3.19	80.8

Number of back-scattered particles = 23

Reflection coefficient = 2.3%

Initial Energy: 10 Kev

Number of Particles: 1000

Particle Number	Back-scattered Energy, Kev	Back-scattering Angle, Degrees
4	1.30	26.2
152	2.18	57.6
335	2.39	36.6
458	1.15	50.2
684	1.12	5.2
689	3.27	70.3
703	2.67	64.8
794	1.28	47.1
803	1.19	69.2
925	1.49	46.4

Number of back-scattered particles = 10

Reflection coefficient = 1.0%

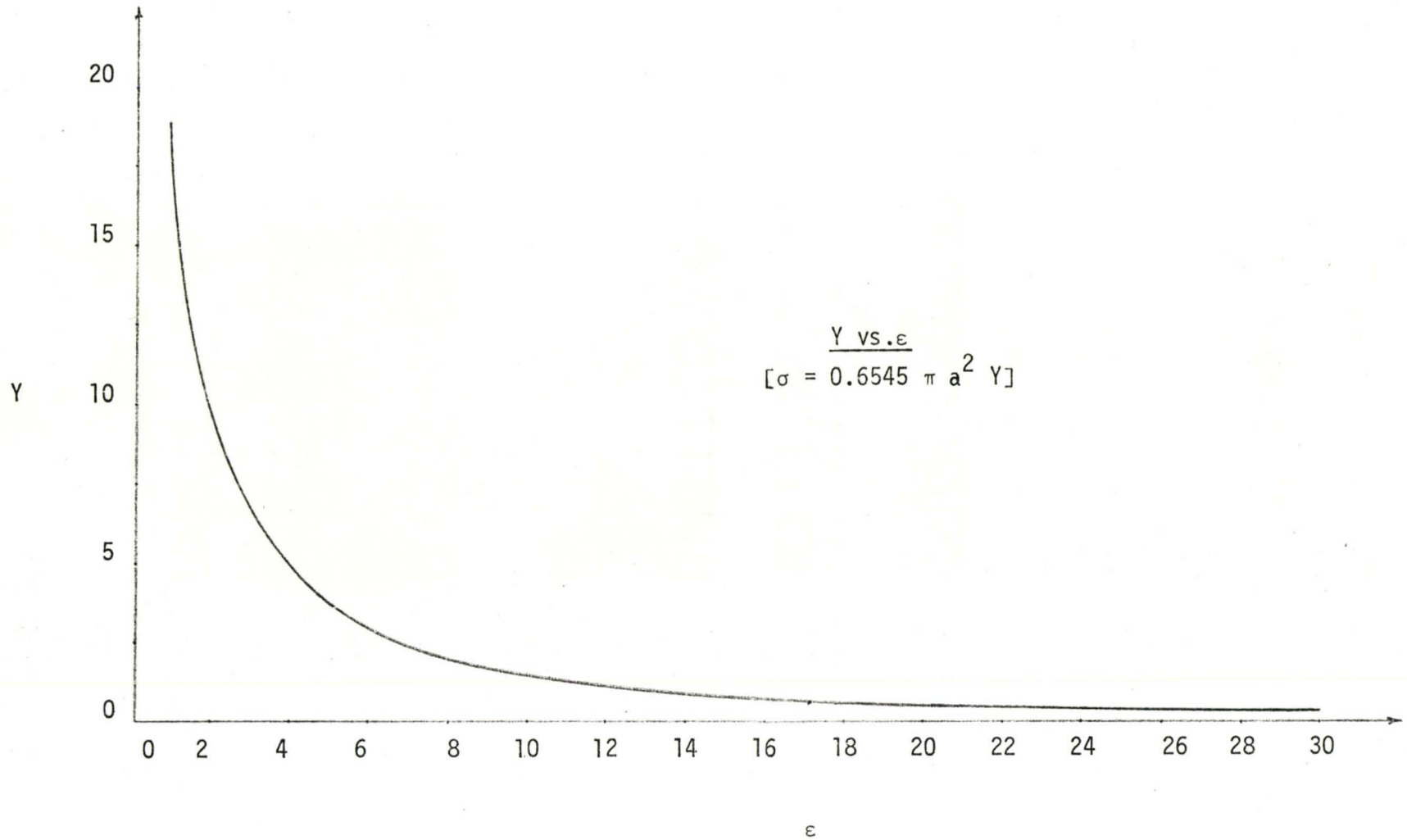
Y vs. ε
[σ = 0.6545 π a² Y]
Y
20
15
10
5
0
0 2 4 6 8 10 12 14 16 18 20 22 24 26 28 30
ε

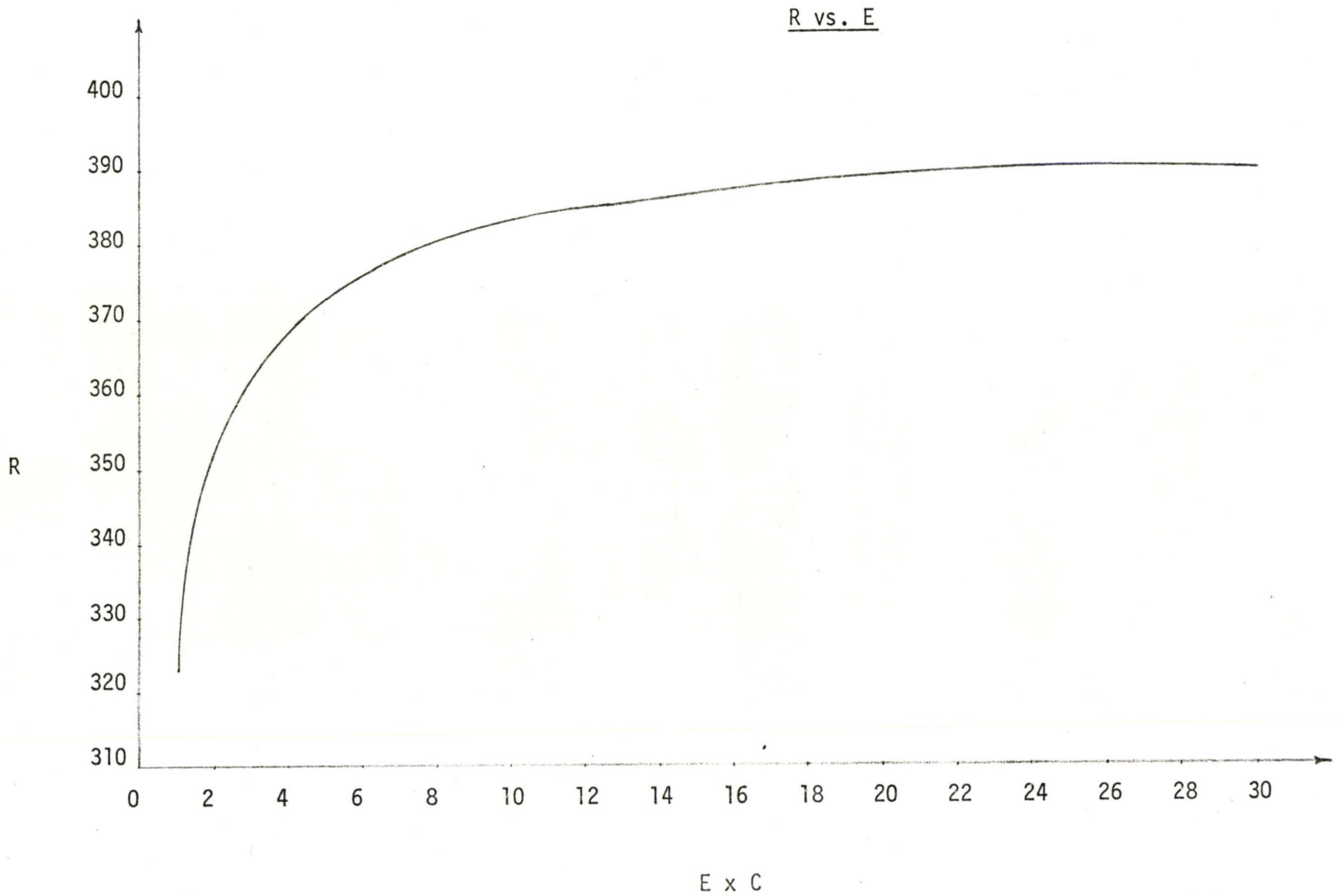
R vs. E
400
390
380
370
360
350
340
330
320
310
R
0
2
4
6
8
10
12
14
16
18
20
22
24
26
28
30
E x C

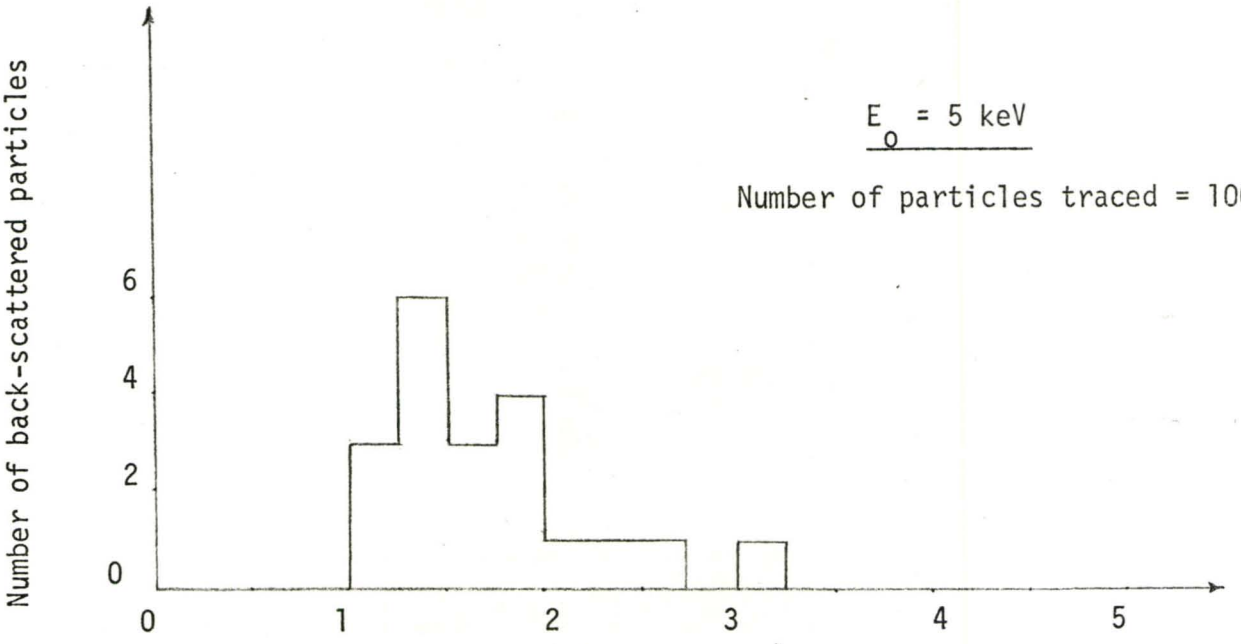
Number of back-scattered particles
E_o = 5 keV
Number of particles traced = 1000
0
2
4
6
0
1
2
3
4
5
Back-scattered Energy, (keV) [greater than 1 keV]

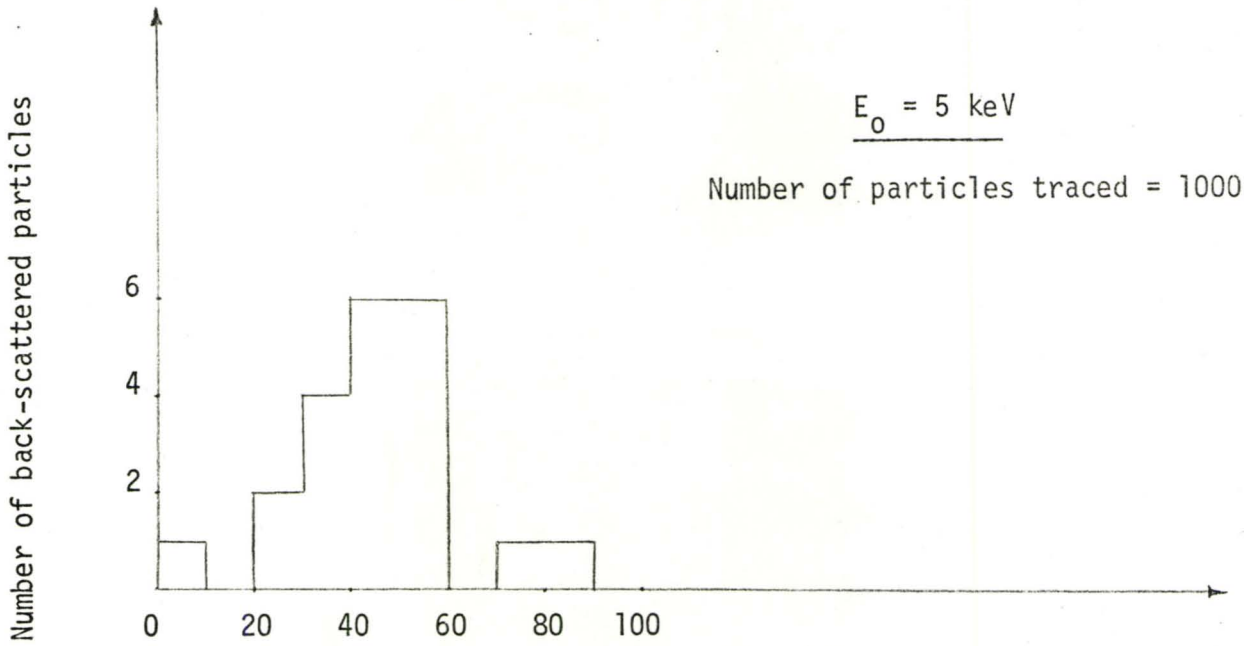
Number of back-scattered particles
E_o = 5 keV
Number of particles traced = 1000
0
2
4
6
0
20
40
60
80
100
Back-scattering angle, (degrees) for particles with energies > 1 keV

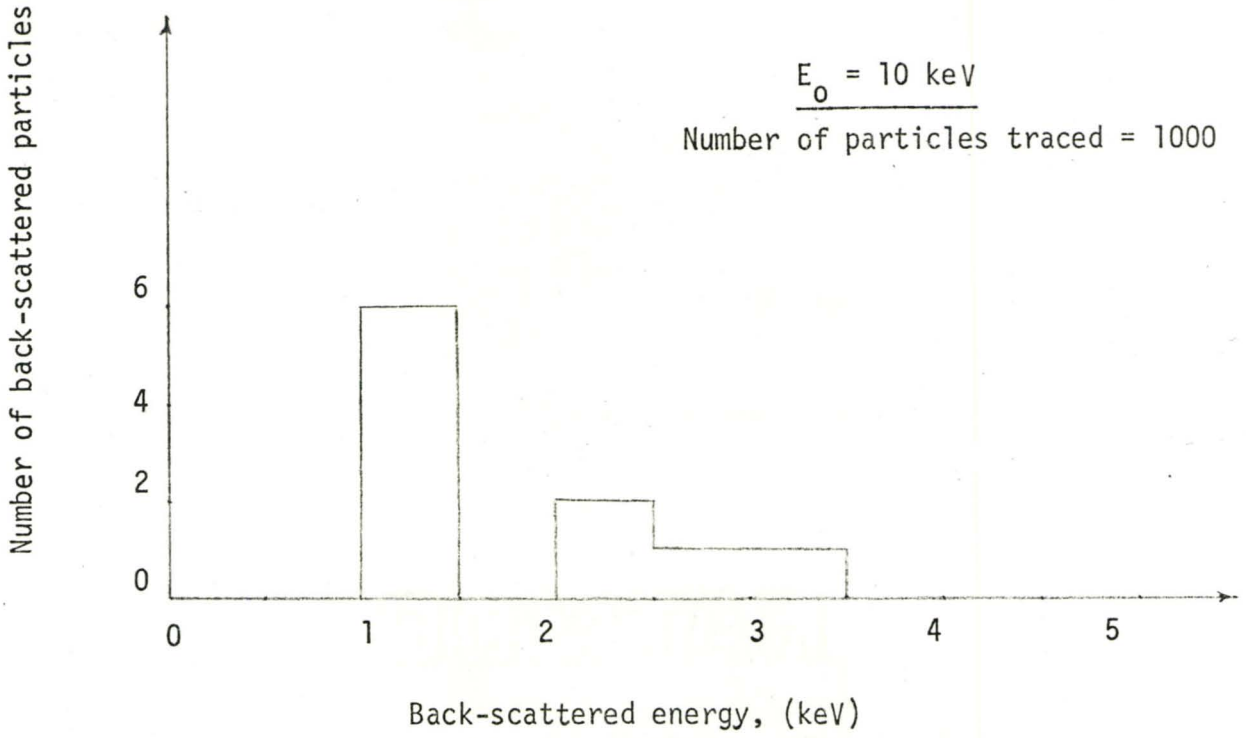
Number of back-scattered particles
E_o = 10 keV
Number of particles traced = 1000
6
4
2
0
0
1
2
3
4
5
Back-scattered energy, (keV)

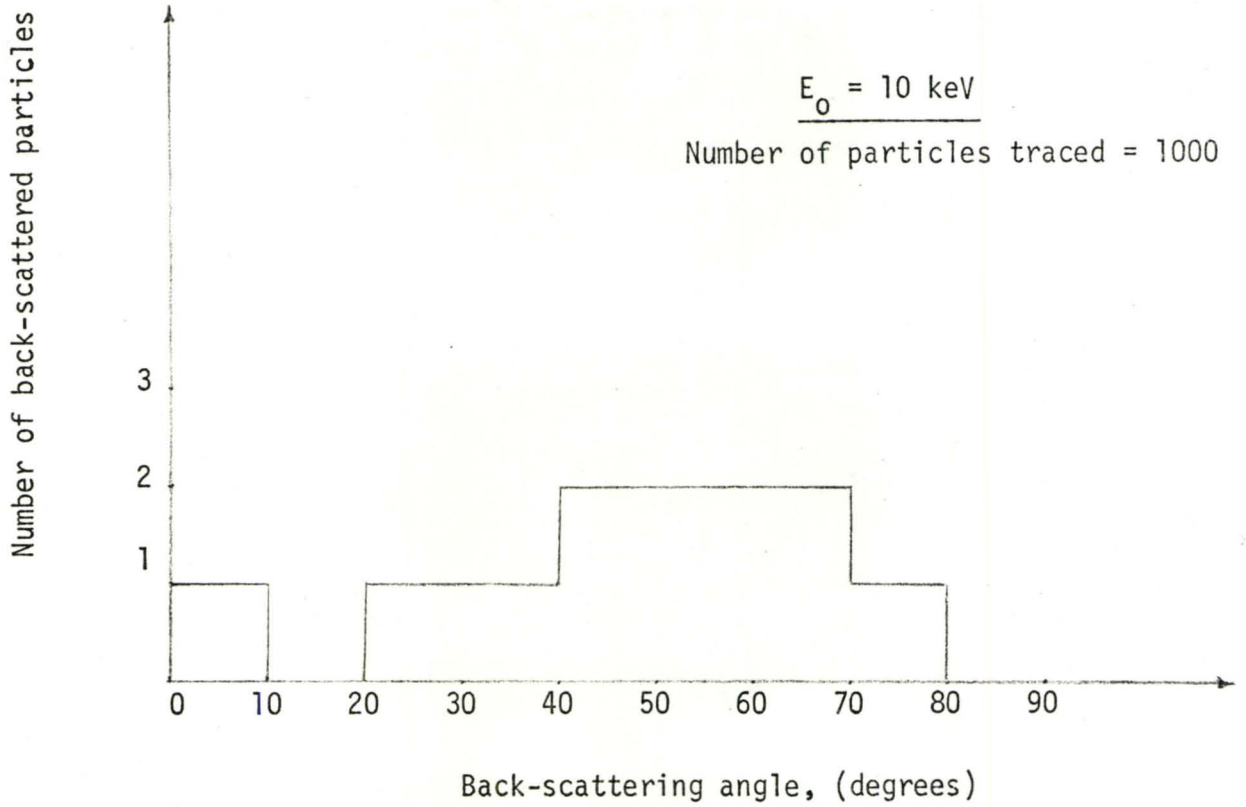
Number of back-scattered particles
E_o = 10 keV
Number of particles traced = 1000
3
2
1
0
10
20
30
40
50
60
70
80
90
Back-scattering angle, (degrees)

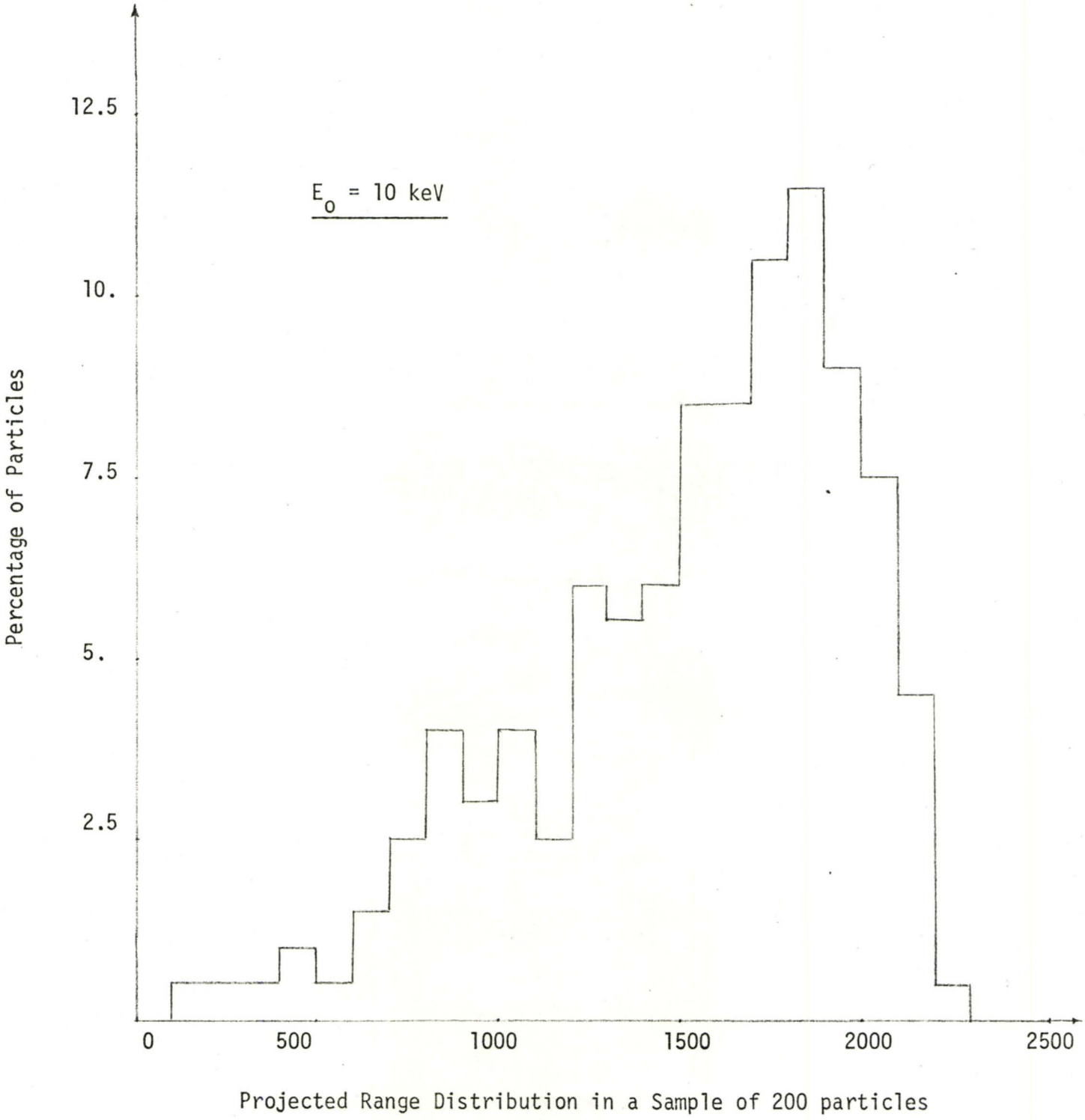
12.5
10.
7.5
5.
2.5
Percentage of Particles
E_o = 10 keV
0
500
1000
1500
2000
2500
Projected Range Distribution in a Sample of 200 particles

4.2 Conclusion

A computer code utilizing three random numbers for collision distance and scattering angles (θ,ϕ) has been developed for light ion penetration and scattering on random targets. The average projected range and straggling are in good agreement with the results of Schiott (1966). However, we have very approximate statistics here since only 200 particles are considered.

The computation time utilized on the CDC-6400 machine is large. We have approximately 10 collisions computed per sec. We could increase the collision computation rate if we fitted the tables of "R" to a polynomial exapnsion.

APPENDIX

```
      PROGRAM TST(INPUT,OUTPUT,PUNCH,TAPE5=INPUT,TAPE6=OUTPUT,TAPE7=PUNC
     1H)
C     CALCULATION OF Y AND R
      EXTERNAL FUN
      COMMON EPS
      DIMENSION          E(400),Y(400),F(400),E1(30),X(30),R(30)
C     CALCULATION OF REDUCED CROSS SECTION
      READ(5,1)  A1,A2,Z1,Z2
      Z=(Z1**(2./3.)+Z2**(2./3.))**(3./2.)
C     A IS THE SCREENING RADIUS
      A=0.8853*0.529*1.E-08*Z**(-1./3.)
      C1=A2/(A1+A2)*A/(Z1*Z2*(4.8*1.E-10)**2)
      C=C1*1.6021*1.E-09
C     EPS=C*E
      C2=0.6545*0.8853**2*0.529*1.E-08*(25.*1.6021*1.E-09)**0.5/(8.*(4.8
     1*1.E-10)**2)*(Z1**(2./3.)+Z2**(2./3.))**0.5/(Z1**(7./6.)*Z2)
      N=0
      J=0
      DEPS1=0.01
      DEPS2=0.1
      EPS=0.
      XL1=0.001
      XL2=0.01
      XL3=0.1
      XU1=0.01
      XU2=0.1
      XU3=1.
      DIV1=40.
      DIV2=80.
      DIV3=80.
      DO 100  I=1,100
      EPS=EPS+DEPS1
      J=J+1
      CALL SIMPS (FUN,XL1,XU1,DIV1,Y1)
      CALL SIMPS (FUN,XL2,XU2,DIV2,Y2)
      CALL SIMPS (FUN,XL3,XU3,DIV3,Y3)
      Y(J)=Y1+Y2+Y3
      N=N+1
      E(N)=EPS/C
      WRITE(6,2)  EPS,E(N),Y(J)
  100 CONTINUE
      J=100
      N=100
      DO 200  I=101,400
      EPS=EPS+DEPS2
      J=J+1
      N=N+1
      CALL SIMPS (FUN,XL1,XU1,DIV1,Y1)
      CALL SIMPS (FUN,XL2,XU2,DIV2,Y2)
      CALL SIMPS (FUN,XL3,XU3,DIV3,Y3)
      Y(J)=Y1+Y2+Y3
      E(N)=EPS/C
      WRITE(6,2)  EPS,E(N),Y(J)
  200 CONTINUE
      WRITE(6,3)
```

```
C       TABULATION OF R FOR DIFFERENT ENERGIES
        DO 300   I=1,400
  300 F(I)=Y(I)/(E(I)*1.6021*1.E-09)**0.5
        J=1
        ODD=0.
        EVEN=0.
        DO 1     I=3,99,2
   10 EVEN=EVEN+F(I)
        DO 20    I=4,98,2
   20 ODD=ODD+F(I)
        X(J)=(E(3)-E(2))*1.6021*1.E-09/3.*(F(2)+4.*EVEN+2.*ODD+F(100))
        DO 40    I=100,390,10
        J=J+1
        ODD=0.
        EVEN=0.
        K=I+1
        L=I+9
        DO 30    I1=K,L,2
   30 EVEN=EVEN+F(I1)
        M=I+2
        N=I+8
        DO 40    I2=M,N,2
   40 ODD=ODD+F(I2)
  400 X(J)=X(J-1)+(E(I+1)-E(I))*1.6021*1.E-09/3.*(F(I)+4.*EVEN+2.*ODD+F(
     1I+10))
        DO 500   I=1,30
  500 R(I)=C2*X(I)
        JJ=0
        DO 600   I=100,390,10
        JJ=JJ+1
  600 E1(JJ)=E(I)
        WRITE(6,4)   (E1(I),I=1,30)
        WRITE(6,3)
        WRITE(6,4)   (R(I),I=1,30)
        WRITE(7,5)   (E(I),I=1,400)
        WRITE(7,5)   (Y(I),I=1,400)
        WRITE(7,6)   (E1(I),I=1,30)
        WRITE(7,6)   (R(I),I=1,30)
    1 FORMAT(2F10.7,2F4.1)
    2 FORMAT(3(5X,E12.6)/)
    3 FORMAT(//)
    4 FORMAT(5X,E12.6/)
    5 FORMAT(6E12.6)
    6 FORMAT(E12.6)
        STOP
        END
```

```
      PROGRAM TST (INPUT,OUTPUT,TAPE5=INPUT,TAPE6=OUTPUT)
C     MONTE CARLO CALCULATIONS OF HYDROGEN IONS BACK-SCATTERING
C     USING THOMAS-FERMI INTERACTION POTENTIAL
C     CONSIDERING BOTH ELECTRONIC AND NUCLEAR SCATTERING
      EXTERNAL FUN
      COMMON EPS
      DIMENSION  R(30),E(30),X(51),Y(51),E1(400),Y1(400),EPSI(2),D(2),
     1PR(2)
      READ(5,1)  A1,A2,Z1,Z2,RHO
      PI=3.14159265
      EPS=C*E
C     SR IS THE SCREENING RADIUS
      SR=0.8853*0.529*.1E-07/(Z1**(2./3.)+Z2**(2./3.))**0.5
      C=A2/(A1+A2)*SR/(Z1*Z2*(4.8*.1E-09)**2)
C     (DE/DX) FOR ELECTRONIC ENERGY LOSS=FK*E**0.5
C     AD IS ATOMIC DENSITY OF TARGET MATERIAL
C     AV IS AVOGADROS NUMBER
      AV=0.602252*.1E+25
      AD=RHO*AV/A2
      FK=8.*PI*AD*(4.8*.1E-09)**2*.529*.1E-07/(25.*1.6021*.1E-08)**0.5*
     1Z1**(7./6.)*Z2/(Z1**(2./3.)+Z2**(2./3.))**(3./2.)
      READ(5,4)  (R(I),I=1,30),(E(I),I=1,30)
      READ(5,8)  (E1(I),I=1,400)
      READ(5,8)  (Y1(I),I=1,400)
C     ************************************************************
C     BACK-SCATTERING CALCULATIONS.
C     ************************************************************
      A=A2/A1
      ALPHA=((A-1.)/(A+1.))**2
      EI1=35.
      DO 1000  II=1,6
      EI1=EI1-5.
      WRITE(6,2)  EI1
      WRITE(6,3)
      M=0
      CALL FRANDN (RN1,1,2)
      DO 400  N=1,1000
      WRITE(6,5) N
      WRITE(6,3)
      NN=0
      EI=EI1
      K=1
      J=1
      EPSI(1)=0.
      EPSI(2)=0.
      PHI=0.
      PR(J)=0.
C     EPSI SCATTERING ANGLE IN LAB SYSTEM
C     PHI AZIMUTHAL ANGLE
C     PR PROJECTED RANGE
  500 DO 800  I=1,30
      IF(EI-E(I))  802,801,800
  800 CONTINUE
  801 EI=E(I)
      R0=R(I)
```

```
      GO TO 803
  802 R0=R(I-1)+(R(I)-R(I-1))/(E(I)-E(I-1))*(EI-E(I-1))
  803 J=J+1
      CALL FRANDN (RN1,1,0)
      IF(RN1.EQ.1.)  GO TO 400
      DELR=ALOG(1.-RN1)
      R1=R0+DELR
      DO 600  I=1,30
      IF(R1-R(I))  602,601,600
  600 CONTINUE
  601 R1=R(I)
      EB=E(I)
      GO TO 603
  602 EB=E(I-1)+(E(I)-E(I-1))/(R(I)-R(I-1))*(R1-R(I-1))
  603 EPS=C*EB*1.6021*.1E-08
      DO 121 I=1,400
      IF(EB-E1(I))  123,122,121
  121 CONTINUE
  122 EB=E1(I)
      Y1B=Y1(I)
      GO TO 124
  123 Y1B=Y1(I-1)+(Y1(I)-Y1(I-1))/(E1(I)-E1(I-1))*(EB-E1(I-1))
  124 D(K)=2.*(1.6021*.1E-08)**.5/EK*(SQRT(EI)-SQRT(EB))
C     D(K) IS ACTUAL DISTANCE TRAVERSED BY ION
      PR(J)=PR(J-1)+D(K)*(COS(EPSI(1))*COS(EPSI(2))+SIN(EPSI(1))*SIN(EPS
     1I(2))*COS(PHI))
      WRITE(6,6)  PR(J)
C     Q1=COS(EPSI(1))
      Q1=COS(EPSI(1))*COS(EPSI(2))+SIN(EPSI(1))*SIN(EPSI(2))*COS(PHI)
      Q2=SIN(EPSI(1))*COS(EPSI(2))+COS(EPSI(1))*SIN(EPSI(2))*COS(PHI)
      IF(Q1)  39,33,39
   33 EPSI(1)=PI/2.
      GO TO 18
   39 IF(Q1.NE.1.0.AND.Q1.NE.-1.0)  GO TO 17
      IF(Q1.NE.1.0)  GO TO 43
      EPSI(1)=0.
      GO TO 18
   43 EPSI(1)=PI
      GO TO 18
   17 EPSI(1)=ATAN(((1.-Q1**2)/Q1**2)**.5)
      IF(Q1.GT.0.)  GO TO 18
      IF(Q2)  38,37,37
   37 EPSI(1)=PI-EPSI(1)
      GO TO 18
   38 EPSI(1)=PI+EPSI(1)
   18 IF(PR(J))  22,22,23
   22 M=M+1
C     BACK-SCATTERING ANGLE IS EPSI(1)
      DS=-PR(J-1)/COS(EPSI(1))
      DS=ABS(DS)
C     DS IS THE DISTANCE TO THE SURFACE
      EBK=(SQRT(EI*1.6021*.1E-08)-0.5*EK*DS)**2/(1.6021*.1E-08)
C     EBK BACK-SCATTERING ENERGY
      BA=EPSI(1)*180./PI
      BA=180.-BA
```

```
C       BA IS THE BACK-SCATTERING ANGLE IN DEGREES
        WRITE(6,9)   EBK,BA
        WRITE(6,3)
        WRITE(6,11)   NN
        WRITE(6,3)
        GO TO 400
     23 IF(EB.GT.1.)  GO TO 180
        GO TO 400
    180 CALL FRANDN (RN2,1,0)
C       CALCULATION OF SCATTERING ANGLE IN C.M. SYSTEM
        RI=RN2*Y1B
C       RI IS PROPORTIONAL TO INTERACTION RATE
        Y(1)=0.
        X(1)=0.001
        XL=0.001
        DIV1=10.
        DIV2=20.
        DIV3=20.
        X(11)=0.01
        X(31)=0.1
        X(51)=1.
        DX1=(X(11)-X(1))/DIV1
        DX2=(X(31)-X(11))/DIV2
        DX3=(X(51)-X(31))/DIV3
        DO 110   I=2,11
        X(I)=X(I-1)+DX1
        XU=X(I)
        CALL SIMPS (FUN,XL,XU,4.,Y(I))
        Y(I)=Y(I-1)+Y(I)
        XL=XU
        IF(RI.LE.Y(I))  GO TO 140
    110 CONTINUE
        DO 120   I=12,31
        X(I)=X(I-1)+DX2
        XU=X(I)
        CALL SIMPS (FUN,XL,XU,4.,Y(I))
        Y(I)=Y(I-1)+Y(I)
        XL=XU
        IF(RI.LE.Y(I))  GO TO 140
    120 CONTINUE
        DO 130   I=32,51
        X(I)=X(I-1)+DX3
        XU=X(I)
        CALL SIMPS (FUN,XL,XU,4.,Y(I))
        Y(I)=Y(I-1)+Y(I)
        XL=XU
        IF(RI.LE.Y(I))  GO TO 140
    130 CONTINUE
    140 DO 700   I=1,51
        IF(RI-Y(I))  702,701,700
    700 CONTINUE
    701 RI=Y(I)
        FT=X(I)
        GO TO 703
    702 FT=X(I-1)+(X(I)-X(I-1))/(Y(I)-Y(I-1))*(RI-Y(I-1))
```

```
C       FT=(T/TMAX) IS FRACTION OF MAXIMUM ENERGY TRANSFERRED
  703   IF(FT.NE.1.0)  GO TO 57
        THETA=PI
        GO TO 58
   57   THETA=2.*ATAN((FT/(1.-FT))**.5)
   58   Q=(A*COS(THETA)+1.)/(A**2+2.*A*COS(THETA)+1.)**.5
        IF(Q)  19,53,19
   53   EPSI(K)=PI/2.
        GO TO 83
   19   IF(Q.NE.1.0.AND.Q.NE.-1.0)  GO TO 63
        IF(Q.NE.1.0)  GO TO 77
        EPSI(K)=0.
        GO TO 83
   77   EPSI(K)=PI
        GO TO 83
   63   EPSI(K)=ATAN(((1.-Q**2)/Q**2)**.5)
   83   EI=EB*(1.-(1.-ALPHA)*FT)
C       EI PARTICLE ENERGY AFTER NUCLEAR COLLISION
        NN=NN+1
        IF(EI.GT.1.)  GO TO 170
        GO TO  400
  170   CALL FRANDN (RN3,1,0)
        AK=FLOAT(K)
        PHI=2.*PI*RN3*(AK-1.)
        K=2
        PR(J-1)=PR(J)
        J=1
        GO TO 500
  400   CONTINUE
        WRITE(6,7)  M
        WRITE(6,3)
 1000   CONTINUE
    1   FORMAT(2F10.7,2F4.1,F6.3)
    2   FORMAT(5X,*INITIAL ENERGY=*,F5.2)
    3   FORMAT(//)
    4   FORMAT(E12.6)
    5   FORMAT(5X,*PARTICLE NUMBER    *,I4)
    6   FORMAT(5X,E12.6)
    7   FORMAT(5X,*NUMBER OF BACK-SCATTERED PARTICLES=*,I4)
    8   FORMAT(6E12.6)
    9   FORMAT(5X,*BACK-SCATTERED ENERGY=*,E12.6,5X,*BACK-SCATTERING ANGLE
       1=*,F8.4/)
   11   FORMAT(5X,*NUMBER OF COLLISIONS     *,I3)
        STOP
        END
```

```
      SUBROUTINE SIMPS(FUN,XL,XU,DIV,Y)
      H=(XU-XL)/DIV
      X=XL
      Y=0.
      NUM=DIV/2.
      DO 1 I=1,NUM
      Y=Y+H/3.*(FUN(X)+4.*FUN(X+H)+FUN(X+2.*H))
    1 X=X+2.*H
      RETURN
      END
```

```
      FUNCTION FUN(X)
      COMMON EPS
      X1=EPS**(-2./3.)*X**(-4./3.)
      X2=(2.618*EPS**(4./3.)*X**(2./3.))**(2./3.)
      X3=(1.+X2)**(-3./2.)
      FUN=X1*X3
      RETURN
      END
```

References

1. J. Bottiger, J.A. Davies, P. Sigmund and K.B. Winterborn, "On the Reflection Coefficient of Kev Heavy-Ion Beams From Solid Targets", Radiation Effects, Vol. 11, (1971)
2. G. Carter and J.S. Colligon, "Ion Bombardment of Solids", American Elsevier Publishing Company, Inc. (1968)
3. K. Güttner, H. Ewald and H. Schmidt, "Monte-Carlo Calculations of the Back-scattering of High-energy Heavy Ions from Metal Surfaces", Radiation Effects, Vol. 13 (1972)
4. J. Linhard and M. Scharff, "Energy Dissipation by Ions in the Kev Region", Phys. Rev., Vol. 124, No.1, (1961)
5. J. Linhard, V. Nielsen and M. Scharff, "Approximation Method in Classical Scattering by Screened Coulomb Fields (notes on Atomic Collisions I), Mat. Fys. Medd. Dan. Vid. Selsk., Vol. 36, No.10 (1968)
6. G.M. McCracken and N.J. Freeman, "Back-scattering of Kev Hydrogen Ions in Solids", J. Phys. B (Atom. Molec. Phys.), Ser. 2, Vol. 2 (1969)
7. O.S. Oen, D.K. Holmes and Mark T. Robinson, "Ranges of Energetic Atoms in Solids", J. Appl. Phys., Vol. 34, No.2 (1963)
8. O.S. Oen and Mark T. Robinson, "Monte-Carlo Range Calculations for a Thomas-Fermi Potential", J. Appl. Phys., Vol. 35, No.8 (1964)
9. H.E. Schiott, Kgl. Dansk Videnskab-Selskab Mat.-Fys., Medd. 35, No.9 (1966)
10. A.V. Wijngaarden, B. Miremadi and W.E. Baylis, "Energy Spectra of Kev Back-scattered Protons as a Probe for Surface-Region Studies", Can. J. Phys., Vol. 49 (1971)

11. K.B. Winterborn, P. Sigmund and J.B. Sanders, "Spatial Distribution of Energy Deposited by Atomic Particles in Elastic Collisions", Det. Kong, Dans. Vid. Sels. Mat-Fys. Medd. 87, 14 (1970)